NASA Technical Paper 1189

Aerodynamic Characteristics at Mach Number 0.2 of a Wing-Body Concept for a Hypersonic Research Airplane

James L. Dillon and Theodore R. Creel, Jr.

JUNE 1978

NASA

NASA Technical Paper 1189

Aerodynamic Characteristics at Mach Number 0.2 of a Wing-Body Concept for a Hypersonic Research Airplane

James L. Dillon and Theodore R. Creel, Jr.
Langley Research Center
Hampton, Virginia

National Aeronautics
and Space Administration

**Scientific and Technical
Information Office**

1978

SUMMARY

An experimental investigation of the static aerodynamic characteristics of a model of a wing-body concept for a high-speed research airplane was conducted in the Langley low-turbulence pressure tunnel. The experiment consisted of configuration buildup from the basic body by adding a wing, center vertical tail, three-module scramjet, and six-module scramjet engine. The test Mach number was 0.2 at Reynolds numbers, based on fuselage length, ranging from 2.78×10^6 to 23×10^6. The test angle-of-attack range was approximately -5° to 30° at constant angles of sideslip of 0° and 4°. The elevons were deflected from 5° to -15°. Roll and yaw control were investigated.

The concept was trimmable up to an angle of attack of approximately 16° with a maximum of -15° of elevon deflection. The basic configuration had a trimmed maximum lift-drag ratio $(L/D)_{max}$ of 5.3; addition of the scramjet engine reduced $(L/D)_{max}$ to 3.75. The concept with or without engine installed showed positive effective dihedral at all positive trimmed angles of attack but was statically unstable directionally above an angle of attack of 10°. Roll and yaw control were available with negligible cross coupling over the trimmed angle-of-attack range.

INTRODUCTION

Several studies have been carried out by government and industrial organizations relating to potential air-breathing hypersonic accelerator and cruise vehicles for both civil and military applications. Some of the problems associated with these higher flight speeds include the development and application of new propulsion systems which use nonpetroleum derived fuels such as liquid hydrogen and new structural concepts which can withstand the high aerodynamic heating including insulated tankage for storing cryogenic fuel such as liquid hydrogen under these adverse thermal conditions (ref. 1). One industry study (ref. 2) concluded that both ground facilities and research flight vehicles would be required to develop these new systems. Past experience with research airplanes has shown that the air-launch, rocket-boost, and glide-descent flight technique is an effective means of conducting advanced flight research, and several studies using this technique have been made in recent years.

The design features that are necessary for good hypersonic aerodynamic characteristics in general are not conducive to good subsonic performance. In addition, the subsonic drag associated with the base area necessary to accommodate a rocket exhaust nozzle and with experiments such as the airframe integrated propulsion system makes acceptable performance characteristics during the unpowered approach and landing a critical design area.

The purpose of the present study was to investigate experimentally the subsonic longitudinal, lateral, and directional stability and control characteristics of one Langley developed wing-body concept for a hypersonic research airplane. This particular concept was sized to fit the existing B-52 launch

system, to be rocket boosted to about a Mach number of 6, and to have sufficient volume to accommodate various experiments such as an advanced scramjet propulsion system. The parametric tests included configuration buildup and elevon and rudder deflection. The study was conducted at a Mach number of 0.2 and a Reynolds number range of 2.78×10^6 to 23×10^6, based on fuselage length. The angle of attack varied from about -5° to 30° at constant angles of sideslip of 0° and 4°. Only those data and results pertinent to an overall assessment of this concept at subsonic speeds are presented in the main body of the paper. The basic data are presented in the appendixes. The results from a test at transonic speeds on this same model are reported in reference 3.

SYMBOLS

The longitudinal characteristics are presented about the stability axis, and the lateral-directional characteristics are presented about the body axis (fig. 1). The moment reference point was at the design center-of-gravity location which was 65 percent of the body length longitudinally and on the model reference line vertically (fig. 2). Values are given in SI units. (Table I presents values in both SI and U.S. Customary Units.) Measurements and calculations were made in U.S. Customary Units.

A_b base area of fuselage, meter^2

A_r reference area, 0.0626 meter^2

$\frac{A_{rudder}}{A_{total}}$ ratio of rudder area to total vertical-tail area

b wing span, meters

C_A axial-force coefficient, $\frac{F_A}{q_\infty A_r}$

C_D drag coefficient, $\frac{D}{q_\infty A_r}$

$C_{D,b}$ base-drag coefficient, $\frac{\text{Base drag}}{q_\infty A_r}$

$C_{D,o}$ drag coefficient at zero lift $(C_D)_{C_L=0}$ (obtained by extrapolating C_D plotted against C_L^2 to $C_L = 0$)

C_L lift coefficient, $\frac{L}{q_\infty A_r}$

C_{L_α} lift-curve slope, $\frac{\partial C_L}{\partial \alpha}$, per degree

C_l rolling-moment coefficient, $\frac{M_X}{q_\infty A_r b}$

C_{l_β} effective-dihedral parameter $\frac{\Delta C_l}{\Delta \beta}$ obtained from values of C_l at $\beta \approx 0^\circ$ and 4°, per degree

$C_{l_{\delta_h}}$ rate of change of C_l with differential elevon deflection, $\left[(C_l)_{\delta_h=20} - (C_l)_{\delta_h=0}\right]/20$, per degree

$C_{l_{\delta_v}}$ rate of change of C_l with rudder deflection, per degree

C_m pitching-moment coefficient, $\frac{M_Y}{q_\infty A_r \ell}$

$C_{m,o}$ pitching-moment coefficient at zero lift

C_{m_α} pitching-moment curve slope, $\frac{\partial C_m}{\partial \alpha}$, per degree

$\partial C_m / \partial C_L$ static longitudinal-stability parameter, based on ℓ

C_N normal-force coefficient, $\frac{F_N}{q_\infty A_r}$

C_n yawing-moment coefficient, $\frac{M_Z}{q_\infty A_r b}$

C_{n_β} directional-stability parameter $\frac{\Delta C_n}{\Delta \beta}$ obtained from values of C_n for $\beta \approx 0^\circ$ and 4°, per degree

$C_{n_{\delta_h}}$ rate of change of C_n with differential elevon deflection, $\left[(C_n)_{\delta_h=20} - (C_n)_{\delta_h=0}\right]/20$, per degree

$C_{n_{\delta_v}}$ rate of change of C_n with rudder deflection, per degree

$C_{p,b}$ base-pressure coefficient, $\frac{p_b - p_\infty}{q_\infty}$

C_Y side-force coefficient, $\frac{F_Y}{q_\infty A_r}$

C_{Y_β} side-force parameter $\frac{\Delta C_Y}{\Delta \beta}$ obtained from values of C_Y for $\beta \approx 0^o$ and 4^o, per degree

$C_{Y_{\delta_h}}$ rate of change of C_Y with differential elevon deflection, $\left[(C_Y)_{\delta_h=20} - (C_Y)_{\delta_h=0}\right]/20$, per degree

$C_{Y_{\delta_v}}$ rate of change of C_Y with rudder deflection, per degree

D drag, $F_N \sin \alpha + F_A \cos \alpha$

F_A axial force along X-axis, positive direction -X

F_N normal force along Z-axis, positive direction -Z

F_Y side force along Y-axis, positive direction Y

L lift, $F_N \cos \alpha - F_A \sin \alpha$

ℓ length of model fuselage, meters

L/D lift-drag ratio

M_∞ free-stream Mach number

M_X, M_Y, M_Z moments about X-, Y-, and Z-axes, respectively

p_b base pressure

p_∞ free-stream static pressure

q_∞ free-stream dynamic pressure

R_ℓ Reynolds number based on fuselage length

X, Y, Z reference axes, unsubscripted symbols indicate body axes

α	angle of attack, degrees
β	angle of sideslip, degrees
δ_e	elevon deflection angle, positive when trailing edge is down, degrees

Subscripts:

max	maximum value
o	zero lift conditions
s	stability axis system
t	trim condition, $C_m = 0$
δ_h	differentially deflected ailerons for roll control
δ_v	deflected rudder for yaw control

Model nomenclature:

B	body or fuselage
BF	base fairing
BWV_{CS}	basic configuration
$BWV_{CS}E_{\delta}$	complete configuration
E_3	three-module scramjet engine
E_6	six-module scramjet engine
LG	landing gear
V_{CDB}	center vertical tail, speed brakes
V_{CH}	center vertical tail, hypersonic, wedge airfoil
V_{CS}	center vertical tail, subsonic, diamond airfoil
W	wing

CONCEPT

The overall design rationale for this concept was primarily based on performance, stability, and control requirements at a Mach number range of 6 to 8 and the performance at touchdown speed, with the scramjet engine installed. Reference 4 has shown that vehicle performance is sensitive to the longitudinal location of the scramjet engine and to wing incidence since the engine produces

moments that must be counterbalanced by the wing and elevons. The scramjet engine also dictates the underbody shape of the vehicle since the airframe-integrated scramjet concept uses the forebody for precompressed air and the aftbody for a half-nozzle expansion ramp (ref. 5). A three-module scramjet engine package is considered the minimum number to make a meaningful flight experiment, whereas a six-module package is representative of the size required to produce positive net thrust minus drag at a Mach number of 6. The center vertical tail was designed with a dual hinge line at approximately the two-thirds chord location to allow for a diamond airfoil for subsonic through supersonic speeds, a wedge airfoil for hypersonic speeds, and for speed brake extension. Base fairings were added to determine the effect of reducing the flat base area on drag at touchdown speeds.

This basic configuration is estimated to weigh about 26 535 kg at launch with an empty operating weight of 9752 kg, whereas the six-module scramjet engine would add 2268 kg.

MODEL

The 0.033-scale test model was of modular design to permit buildup of the basic model (fig. 2(a)) from components consisting of body, cropped delta wing, center vertical tail, base fairings, scramjet engine, and landing gear. The wing had 2.1° negative incidence and 10° dihedral. The airfoil was a modified circular arc with a leading-edge radius (normal to the leading edge) of 0.064 cm followed by a 10° wedge section, and the elevons had a constant thickness at the hinge line of 0.814 cm and 7.6° wedge angle. The top and bottom surfaces of the elevons were contoured over approximately the aft one-third to give a trailing-edge thickness of 0.064 cm. The elevons could be deflected ±20°. Two model scramjet engine packages consisting of three and six clustered modules were also tested. (See figs. 2(c) and 3.) The proposed flight research engine has three internal fuel struts in each module, whereas the model engine packages used in this test simulated the internal geometric contraction by use of one strut. Tests on a 0.10-scale model of this concept showed that simulation of the internal geometric contraction ratio as was done in this test gives excellent overall vehicle forces and moments relative to the three fuel strut case. (See ref. 6.) The base fairings are shown in figures 2(a) and 3; the vertical tail, in figure 2(b); and the landing gear, in figure 2(d). A photograph of the cast model with its interchangeable parts is shown in figure 3. The pertinent geometrical characteristics of the model for aerodynamic testing are listed in table I.

APPARATUS, TEST, AND CORRECTIONS

Tunnel and Test Conditions

The investigation was conducted in the Langley low-turbulence pressure tunnel (ref. 7). This is a closed-throat, single-return tunnel which can be operated at stagnation pressures from 0.1 to 10 atmospheres. The test section is 91.4 cm wide by 228.6 cm high.

The model was sting mounted with an electrically driven roll coupling in the sting support system. This setup minimizes wall interference effects during sideslip investigation by keeping the model in the center of the test section through a combination of pitch angle and roll angle for a desired α and β test point. The coupling also readily allowed testing the model inverted to acquire data at a more negative angle of attack than the tunnel pitch mechanism would allow if the model were in an upright orientation.

The aerodynamic forces and moments were measured by means of a six-component strain-gage balance which was housed inside the model fuselage and attached to the tunnel sting support system. Base pressure was measured with three forward facing pressure tubes located approximately 0.2 cm behind the fuselage base. All tests were made at $M_\infty = 0.2$ with both free and fixed transition on the model. The limited free-transition tests were conducted over a Reynolds number range of 2.8×10^6 to 23×10^6, based on fuselage length. Most of the tests were conducted with fixed transition at a Reynolds number of 11.5×10^6, based on fuselage length. Transition was fixed for this Reynolds number condition (by use of the method of ref. 8) by applying 0.32-cm-wide strips of No. 220 carborundum grains at the following locations (measured streamwise): 2.92 cm aft of the nose stagnation point; 5-percent local chord aft of the leading edge of the wing, vertical tail, and engine cowling; and 0.51 cm inside the leading edges of the scramjet engine.

Corrections

The free-stream flow conditions were corrected by the method of reference 9 for the effects of model and wake blockage and by the method of reference 10 for lift interference. The drag data have not been corrected for the pressure acting on the flat fuselage base. However, the measured base pressure values were averaged, and typical measured base pressure coefficients are presented in figure 4. No correction was made to the drag data for flow through the scramjet engine. The angles of attack and roll have been corrected for the deflection of the balance and sting under aerodynamic load.

RESULTS AND DISCUSSION

Static Longitudinal Characteristics

Reynolds number effects.- The free-transition longitudinal characteristics for the basic BWV_{CS} and complete $BWV_{CS}E_6$ configurations are presented in figure 5 for the test range of Reynolds number. Note that the Reynolds number variation affects primarily $(L/D)_{max}$ with approximately a 10- and 6-percent change directly proportional to Reynolds number for the BWV_{CS} and $BWV_{CS}E_6$ configurations, respectively. This variation is probably due to more separation losses around the nozzle expansion ramp for the low relative to the high Reynolds number condition. The zero-lift drag as a function of Reynolds number for both the basic and complete configurations is shown in figure 6. These values of drag were established by plotting C_D against C_L^2 and extrapolating linearly to zero lift. The theoretical prediction from the method of

reference 11, assuming turbulent skin friction, is also shown for the BWV_{CS} configuration. For $R_{\ell} > 4 \times 10^6$, the theory predicts the level and the slightly decreasing trend of $C_{D,o}$ with increasing Reynolds number. At the lower Reynolds numbers, the theory overpredicts the data, probably because the flow on the model has not reached a fully turbulent state. However, these results should be considered fortuitous since the $C_{D,o}$ levels for data that have been corrected for base drag are not predicted by the correlation from reference 11 with the base-drag term neglected. For this concept, the theoretical method is apparently underpredicting the contribution of $C_{D,o}$ due to skin friction and pressure drag but overpredicting base drag such that the total level as shown in figure 6 is predicted very well. Predictions for other similar research airplane concepts show the method of reference 11 to be inconsistent (ref. 12). Note that addition of the engine results in an approximately 100-percent increase in $C_{D,o}$.

Configuration buildup and theoretical comparison.- The longitudinal aerodynamic characteristics for the configuration buildup are presented in appendix A.

The vortex-lattice method of reference 13 (with unpublished improvements) was used to predict the aerodynamic characteristics of the fuselage-wing configuration BW only. The prediction method was used by assuming potential flow over the entire planform plus vortex flow over the wing leading edge and side edge (tip). The mean camber lines of the fuselage and the wing were used to determine the local angles of attack that were input for each panel. A comparison of the theoretical prediction with experimental data is presented in figure 7. The theory predicts the data quite well, especially at the lower lift coefficients.

Trim characteristics.- The effect of elevon deflection on the longitudinal characteristics of the basic and complete configurations is presented in appendix B and was used to determine the trimmed aerodynamic characteristics for each configuration. These characteristics for BWV_{CS} and $BWV_{CS}E_6$ are presented in figures 8 and 9, respectively. Note that this concept was trimmable up to an angle of attack of $\sim 16^{\circ}$ with a maximum elevon deflection of -15° and that the basic configuration has a trimmed $(L/D)_{max}$ of 5.3; the addition of the scramjet engine decreases the trimmed $(L/D)_{max}$ to 3.75. Both configurations have static margins of from 3 to 11 percent across the trimmed angle-of-attack range.

The trimmed aerodynamic parameters at these test conditions reflect performance during the critical unpowered landing phase of the flight profile. Assuming a standard day at Dryden Flight Research Center in California, the steady flight, gear-up speed at $(L/D)_{max}$ for the basic configuration BWV_{CS} would be 235 knots and for the complete configuration $BWV_{CS}E_6$ would be 228 knots. At $\alpha = 15^{\circ}$, the speed with and without the engine would be 213 knots and 196 knots, respectively.

Lateral-Directional Characteristics

Lateral-directional stability.- The variations of the lateral coefficients with angle of sideslip for the complete configuration are presented in appendix C. The static lateral-directional stability derivatives for the body buildup were evaluated for $\beta \approx 0^{\circ}$ and $\beta \approx 4^{\circ}$ and are presented in figure 10. The body alone has positive effective dihedral for $5^{\circ} \leq \alpha \leq 15^{\circ}$, but it is directionally stable only at the higher angles of attack. The addition of the wing provides positive effective dihedral at positive α up to $\alpha = 22^{\circ}$, but it negates the directional stability the body alone possessed. The center vertical-tail addition provides directional stability for $\alpha < 10^{\circ}$ and $\alpha > 28^{\circ}$ and also produces lateral stability over the entire test angle-of-attack range. The addition of the six-module engine and the landing gear does not greatly affect the lateral-directional characteristics except at the higher angles of attack. The theoretical estimates of C_{n_β} and C_{Y_β}, utilizing the technique from reference 14, are also shown in the figure. These estimates are for small angles of attack only. This technique computes the aerodynamic forces and moments on asymmetrical planforms through a vortex-lattice method. As used herein, the side view of the appropriate configuration was input with the model reference line as the center line. The estimates agree well with data at the low angles of attack. The static lateral-stability characteristics for this concept appear sufficient for the approach and touchdown angles of attack expected for this class of vehicles, but the directional-stability characteristics appear deficient, and geometrical alterations would probably have to be made.

Roll and yaw control.- Roll control was investigated for the basic and complete configurations, and the results are presented in figure 11. These data were obtained by deflecting the left elevon 10° and the right elevon -10°. The elevon effectiveness for the basic configuration is about constant with negligible cross coupling up to $\alpha \approx 20^{\circ}$, above which elevon effectiveness decreases and cross coupling becomes dominant. The complete configuration has similar roll-control characteristics up to $\alpha \approx 20^{\circ}$, above which the characteristics remain relatively constant.

The yaw-control characteristics were investigated by deflecting the rudder 15.6° for both the BWV_{CS} and $BWV_{CS}E_6$ configurations, and the results are presented in figure 12. The rudder power for the basic configuration is about constant with negligible cross coupling up to $\alpha \approx 20^{\circ}$; at higher angles of attack the rudder power decreased until effective control reversal was encountered and cross coupling became significant. Similar results were obtained for the complete configuration up to $\alpha \approx 20^{\circ}$; at higher angles of attack the rudder power and cross coupling increased slightly.

The unusual behavior that occurred for the basic but not for the complete configuration may be influenced by the pressure field on the lower fuselage expansion ramp and on the fuselage base. A pressure test on a 1/10-scale model of this concept (ref. 6) showed higher pressures on the nozzle expansion ramp with engine off relative to engine on. In addition, the base pressure measured

on each side of the balance cavity during the roll- and yaw-control investigations was affected more at high angles of attack when the engine was off than when the engine was on.

CONCLUSIONS

An analysis of the data from an experimental investigation of a wing-body concept for a hypersonic research airplane at a Mach number of 0.2 and Reynolds numbers of 2.78×10^6 to 23×10^6, based on fuselage length, leads to the following conclusions:

1. The drag at zero lift was almost invariant with Reynolds number for this concept with or without the six-module scramjet engine installed.

2. Addition of the six-module scramjet engine approximately doubled the drag at zero lift.

3. This concept was trimmable up to an angle of attack of approximately 16° with a maximum of -15° of elevon deflection.

4. The basic configuration had a trimmed maximum lift-drag ratio $(L/D)_{max}$ of 5.3, whereas addition of the six-module scramjet engine reduced $(L/D)_{max}$ to 3.75.

5. The concept with or without engine installed exhibited positive effective dihedral at all positive trimmed angles of attack but was statically directionally unstable above an angle of attack of 10°.

6. Roll and yaw control were available with negligible cross coupling through the test angle-of-attack range for the complete configuration and up to an angle of attack of 22° for the basic configuration; severe cross coupling and effective control reversal were encountered at higher angles of attack for the basic configuration.

Langley Research Center
National Aeronautics and Space Administration
Hampton, VA 23665
April 13, 1978

APPENDIX A

CONFIGURATION BUILDUP

The untrimmed longitudinal aerodynamic characteristics for the configuration buildup are presented in figure 13. Addition of the wing to the body significantly altered the lift, drag, and pitching-moment curves with C_{L_α} becoming much more positive and C_{m_α} shifting from positive to negative. Note that the body-wing configuration BW produced curves of C_m and C_L plotted against α which basically had two linear portions. This behavior is characteristic of a clipped delta wing as seen in references 15 and 16. Addition of the vertical tail had little effect on lift but slightly decreased the pitching moment and drag (to be discussed subsequently). The six-module engine slightly increased the lift at low angles of attack, decreased the pitching moment, and increased the drag which resulted in about a one-unit decrease in untrimmed $(L/D)_{max}$. The base fairings had very little effect on the aerodynamic characteristics.

As was mentioned previously, the model was sting mounted with an electrically driven roll coupling in the support mechanism. This setup facilitated readily testing the model at a more negative α than the strut travel limits allowed simply by rolling the model 180° and moving the strut in its normal positive direction. The data from selected configurations in an upright and inverted attitude are presented in figure 14. Note that data were obtained for an overlapping angle-of-attack range, depending on model orientation. All parameters for each configuration agree well in this overlapping region with the exception of BWV_{CS}. The data for this configuration agree well in the overlapping region for lift and pitching moment, but there is an offset in axial force as evidenced more clearly by the larger plot in figure 15. This figure shows that the BWV_{CS} configuration in an inverted attitude had a ΔC_A of approximately 0.0037 compared to the upright case. This ΔC_A has been added to the measured axial-force data for the BWV_{CS} configuration and results in the recommended drag polar characteristics indicated by the dashed-line curve in figure 15. All subsequent drag data and analysis presented in this paper for the BWV_{CS} configuration with $\delta_e = 0°$ are as shown by the dashed-line curve in figure 15. This increment will make the body buildup forces behave as expected; that is, L/D for $BWV_{CS} < BW$.

The effect of the number of engine modules on the aerodynamic characteristics is shown in figure 16. The addition of either the three-module scramjet or the six-module scramjet affects primarily drag (or lift-drag ratio). The lift-drag ratio decreases with increasing modules, but the three-module engine has a slightly greater effect than the six-module engine.

The effect of vertical-tail changes is presented in figure 17. The change from a diamond-shaped subsonic airfoil to a hypersonic wedge shape or to speed brakes by differential rudder deflection affects the lift, drag, and pitching

moment. The tail variations produce a shift in α_o while C_{L_α} remains essentially constant. Likewise, $C_{m,o}$ increases with differential rudder deflection, but the aerodynamic center remains essentially constant. The drag polar shifts with rudder deflection which results in the hypersonic wedge tail and the speed brakes causing a decrement in $(L/D)_{max}$ of approximately 0.4 and 0.9, respectively, relative to the subsonic tail case.

The perturbation deployment of the landing-gear causes is shown in figure 18. The landing gear affects primarily drag with a decrement in $(L/D)_{max}$ of about 0.6.

Figure 19 shows the results from plugging the scramjet engine, that is, blocking off the airflow at the combustor exit. The lift is slightly decreased, the drag essentially unchanged, $C_{m,o}$ increased, and the aerodynamic center unchanged. These results would occur if the pressure on the aft-facing expansion ramp were unchanged by plugging the engine while the spillage characteristics were altered to effect a decrease in pressure on the engine cowl. This flow situation would produce a decrease in lift and, by virtue of the engine location, a noseup pitching moment.

APPENDIX B

EFFECT OF ELEVON DEFLECTION

The effect of elevon deflection on the longitudinal characteristics of the basic and complete configurations is presented in figure 20. These data were used to determine the trimmed longitudinal characteristics for this concept with and without the engine installed.

APPENDIX C

BASIC SIDESLIP CHARACTERISTICS

The basic sideslip characteristics of the $BWV_{CS}E_6$ configuration are presented in figure 21 for $\alpha \sim 1^{\circ}$ ($C_L \sim 0^{\circ}$) and $\alpha \sim 16^{\circ}$. These data were used to determine the linearity of the lateral-directional aerodynamic characteristics. The lateral-directional stability derivatives were obtained from values of the coefficients at $\beta \sim 0^{\circ}$ and $\beta \sim 4^{\circ}$; note that the linearity is good at both angles of attack, especially for $0^{\circ} \leq \beta \leq 4^{\circ}$.

REFERENCES

1. Hearth, Donald P.; and Preyss, Albert E.: Hypersonic Technology - Approach to an Expanded Program. Astronaut. & Aeronaut., vol. 14, no. 12, Dec. 1976, pp. 20-37.

2. Hypersonic Research Facilities Study. Phase III - Final Studies. Volume IV, Part 1 - Flight Research Facilities. NASA CR-114327, 1970.

3. Dillon, James L.; and Pittman, Jimmy L.: Aerodynamic Characteristics at Mach Numbers From 0.33 to 1.20 of a Wing-Body Design Concept for a Hypersonic Research Airplane. NASA TP-1044, 1977.

4. Henry, John R.; and Anderson, Griffin Y.: Design Considerations for the Airframe-Integrated Scramjet. NASA TM X-2895, 1973.

5. Weidner, J. P.; Small, W. J.; and Penland, J. A.: Scramjet Integration on Hypersonic Research Airplane Concepts. AIAA Paper No. 76-755, July 1976.

6. Johnston, Patrick J.; Pittman, Jimmy L.; and Huffman, Jarrett K.: Effect of an Integrated Scramjet Installation on the Subsonic Performance of an Aircraft Designed for Mach 6 Cruise. [Paper] 77-1230, American Inst. Aeronaut. & Astronaut., Aug. 1977.

7. Von Doenhoff, Albert E.; and Abbott, Frank T., Jr.: The Langley Two-Dimensional Low-Turbulence Pressure Tunnel. NACA TN 1283, 1947.

8. Braslow, Albert L.; and Knox, Eugene C.: Simplified Method for Determination of Critical Height of Distributed Roughness Particles for Boundary-Layer Transition at Mach Numbers From 0 to 5. NACA TN 4363, 1958.

9. Herriot, John G.: Blockage Corrections for Three-Dimensional-Flow Closed-Throat Wind Tunnels, With Consideration of the Effect of Compressibility. NACA Rep. 995, 1950. (Supersedes NACA RM A7B28.)

10. Garner, H. C.; Rogers, E. W. E.; Acum, W. E. A.; and Maskell, E. C.: Subsonic Wind Tunnel Wall Corrections. AGARDograph 109, Oct. 1966.

11. USAF Stability and Control Datcom. Contracts AF 33(616)-6460 and F33615-71-C-1298, McDonnell Douglas Corp., Oct. 1960. (Revised Feb. 1972.)

12. Penland, Jim A.; Dillon, James L.; and Pittman, Jimmy L.: An Aerodynamic Analysis of Several Hypersonic Research Airplane Concepts From M = 0.2 to 6.0. [Paper] 78-150, American Inst. Aeronaut. & Astronaut., Jan. 1978.

13. Lamar, John E.; and Gloss, Blair B.: Subsonic Aerodynamic Characteristics of Interacting Lifting Surfaces With Separated Flow Around Sharp Edges Predicted by a Vortex-Lattice Method. NASA TN D-7921, 1975.

14. Luckring, James M.: Some Recent Applications of the Suction Analogy to Asymmetric Flow Situations. Vortex-Lattice Utilization, NASA SP-405, 1976, pp. 219-236.

15. Palmer, William E.: Effect of Reduction in Thickness From 6 to 2 Percent and Removal of the Pointed Tips on the Subsonic Static Longitudinal Stability Characteristics of a 60° Triangular Wing in Combination With a Fuselage. NACA RM L53F24, 1953.

16. Kirby, D. A.: Low-Speed Wind-Tunnel Measurements of the Lift, Drag and Pitching Moment of a Series of Cropped Delta Wings. R. & M. No. 3744, British A.R.C., Nov. 1972.

TABLE I.- GEOMETRIC CHARACTERISTICS OF MODEL

Wing:	
Area (includes fuselage intercept), m^2 (in^2)	0.060 (92.63)
Area, exposed, m^2 (in^2)	0.030 (47.00)
Area, wetted, m^2 (in^2)	0.064 (98.98)
Span, m (in.)	0.244 (9.62)
Aspect ratio	0.999
Root chord (at fuselage center line), m (in.)	0.371 (14.59)
Tip chord, m (in.)	0.119 (4.7)
Taper ratio	0.322
Mean aerodynamic chord (includes fuselage intercept), m (in.)	0.294 (11.57)
Sweepback angles:	
Leading edge, deg	67.5
25-percent chord line, deg	61.1
Trailing edge, deg	0
Dihedral angle, deg	10
Incidence angle, deg	-2.1
Airfoil thickness ratio:	
Exposed root	0.051
Tip	0.078
Leading-edge radius (normal to leading edge), cm (in.)	0.064 (0.025)
Trailing-edge thickness, cm (in.)	0.064 (0.025)
Elevons:	
Tip chord, percent wing tip	36.6
Span, percent total span	59.8
Area, both, m^2 (in^2)	0.0064 (9.89)
Vertical tail:	
Area, exposed, m^2 (in^2)	0.007 (10.93)
Span, exposed, m (in.)	0.077 (3.06)
Aspect ratio of exposed area	0.857
Root chord at fuselage surface line, m (in.)	0.101 (3.99)
Tip chord, m (in.)	0.057 (2.256)
Taper ratio	0.565
Mean aerodynamic chord of exposed area, m (in.)	0.097 (3.804)
Sweepback angles:	
Leading edge, deg	49.9
Trailing edge, deg	18.5
Hinge-line location, percent chord	68.7
A_{rudder}/A_{total}	0.295
Leading-edge radius, cm (in.)	0.064 (0.025)
Fuselage:	
Length, m (in.)	0.584 (23.0)
Nose radius, cm (in.)	0.159 (0.063)
Maximum height, m (in.)	0.076 (2.98)
Maximum width, m (in.)	0.097 (3.83)
Fineness ratio of equivalent round body	6.86
Planform area, m^2 (in^2)	0.042 (65.12)
Wetted area:	
Without components or base, m^2 (in^2)	0.122 (188.6)
With wing on, m^2 (in^2)	0.116 (179.4)
A_b, m^2 (in^2)	0.0023 (3.54)
Complete model:	
Planform area, m^2 (in^2)	0.072 (112.12)
Aspect ratio of planform	0.825

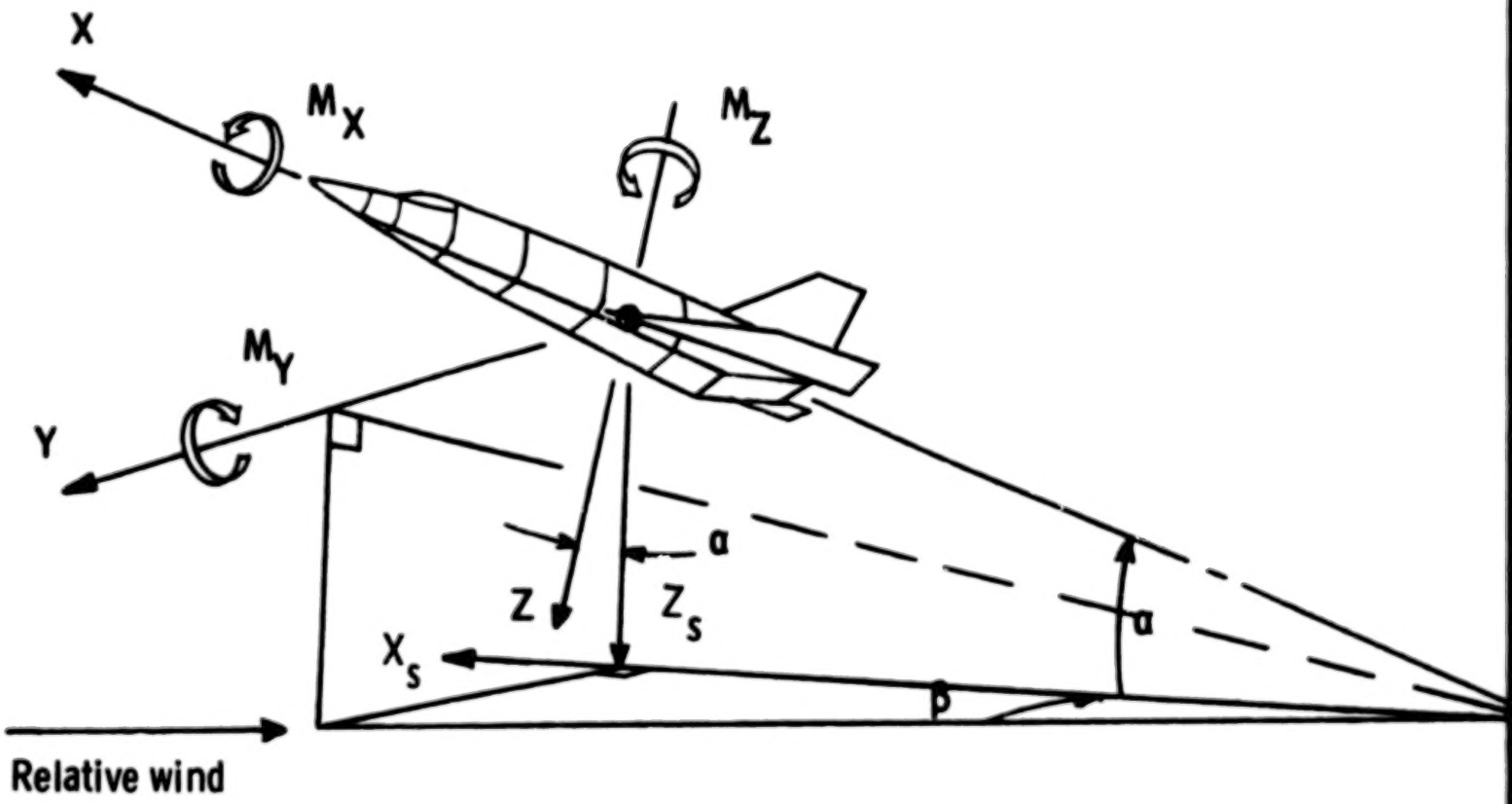

Figure 1.- System of reference axes. Arrows indicate positive directions.

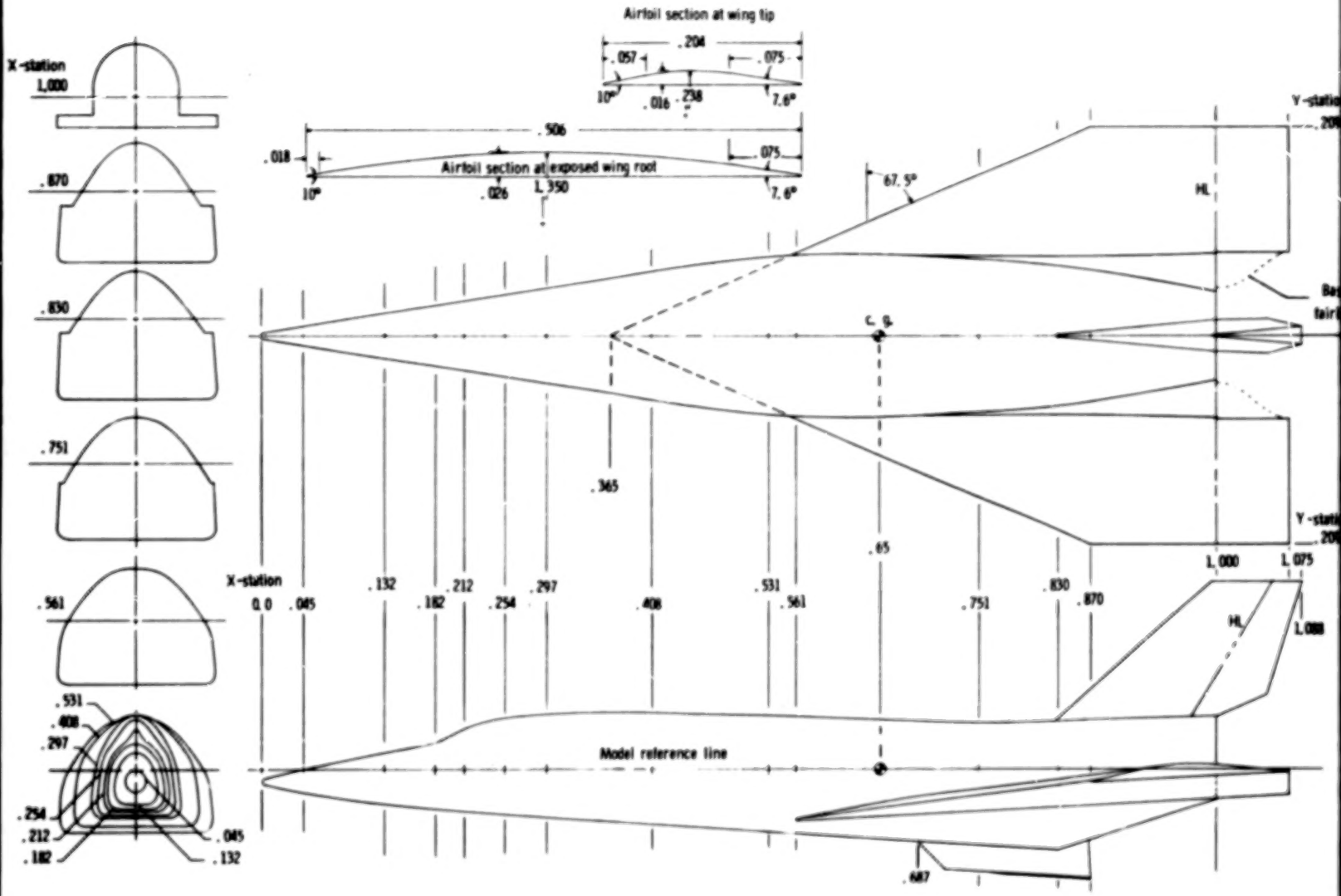

(a) Model details.

Figure 2.- Model general dimensions. All dimensions have been normalized by body length (ℓ = 58.4 cm) unless otherwise noted.

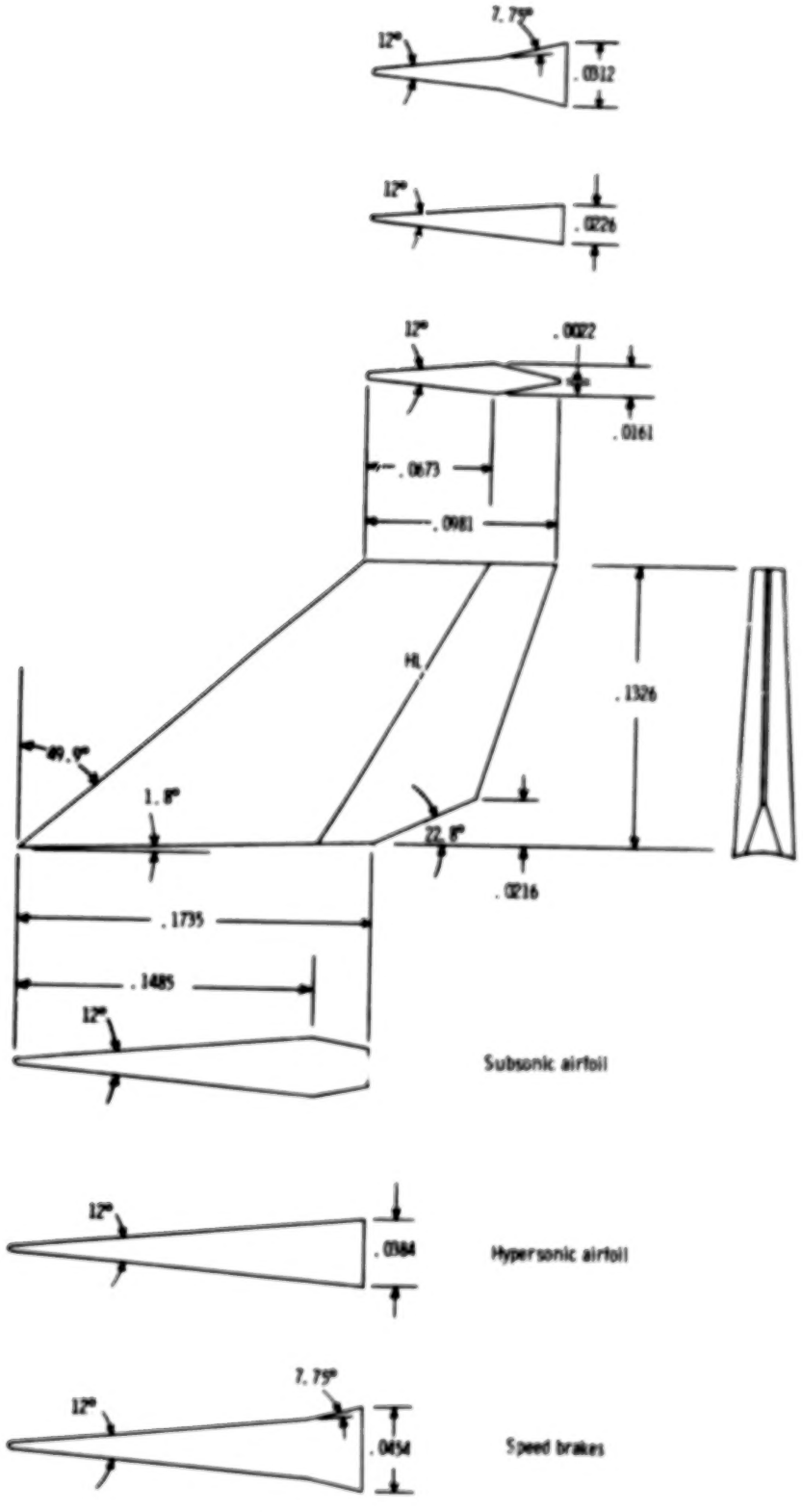

(b) Vertical-tail variations.

Figure 2.- Continued.

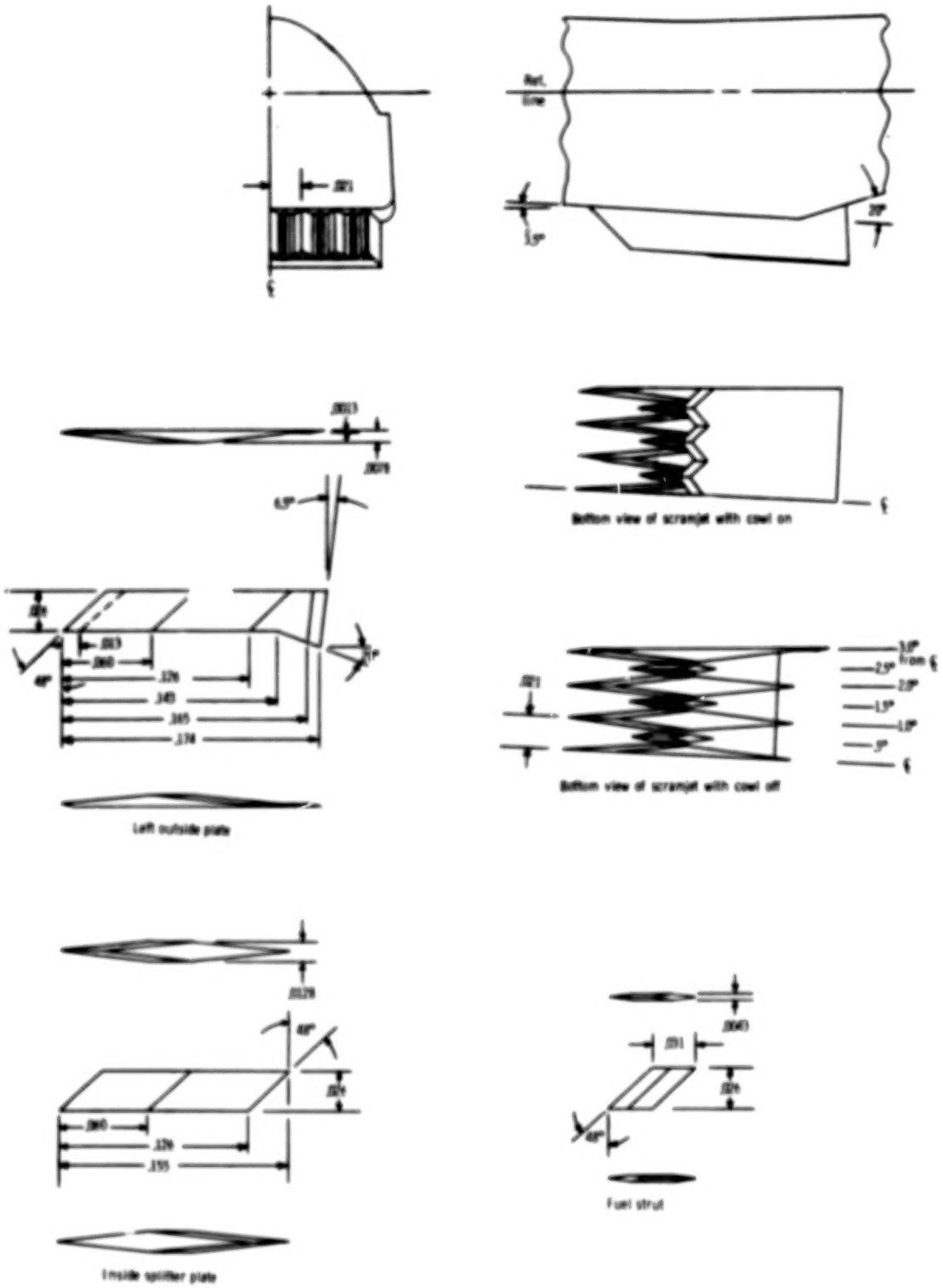

(c) Scramjet-engine details.

Figure 2.- Continued.

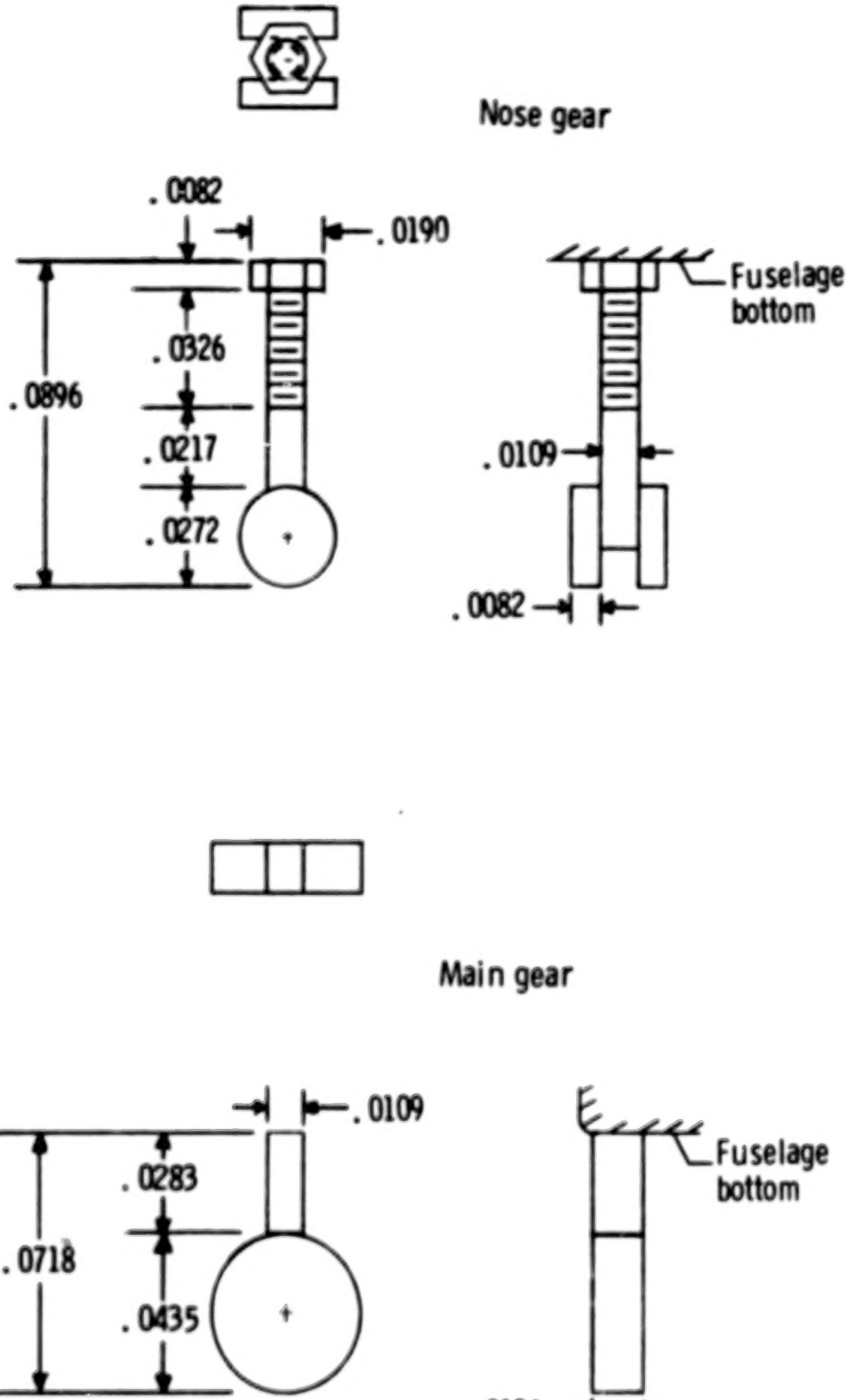

(d) Landing-gear details.

Figure 2.- Concluded.

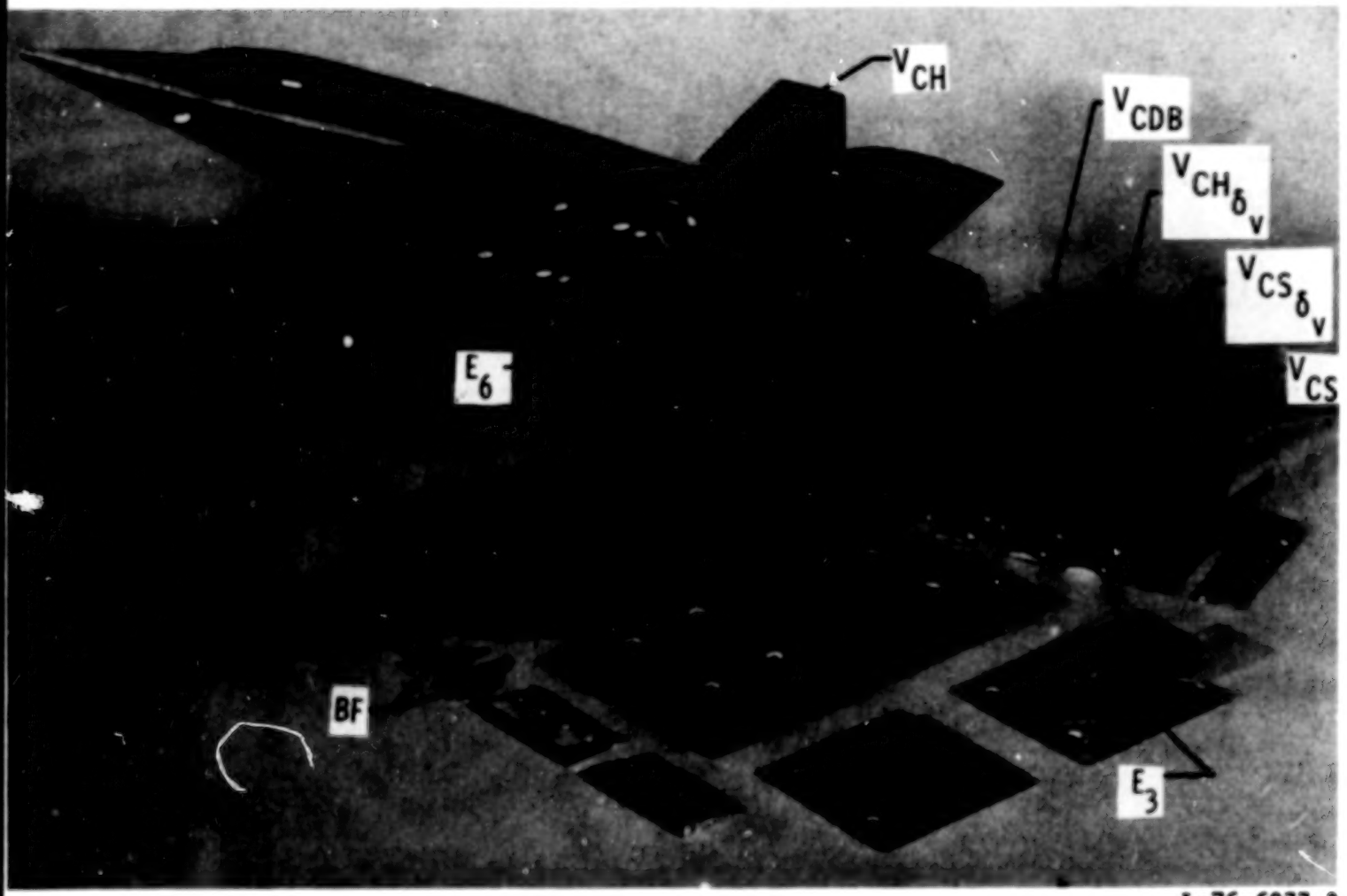

L-76-6977.2

Figure 3.- Photograph of model with various parts. (Note that all components were not used in this test.)

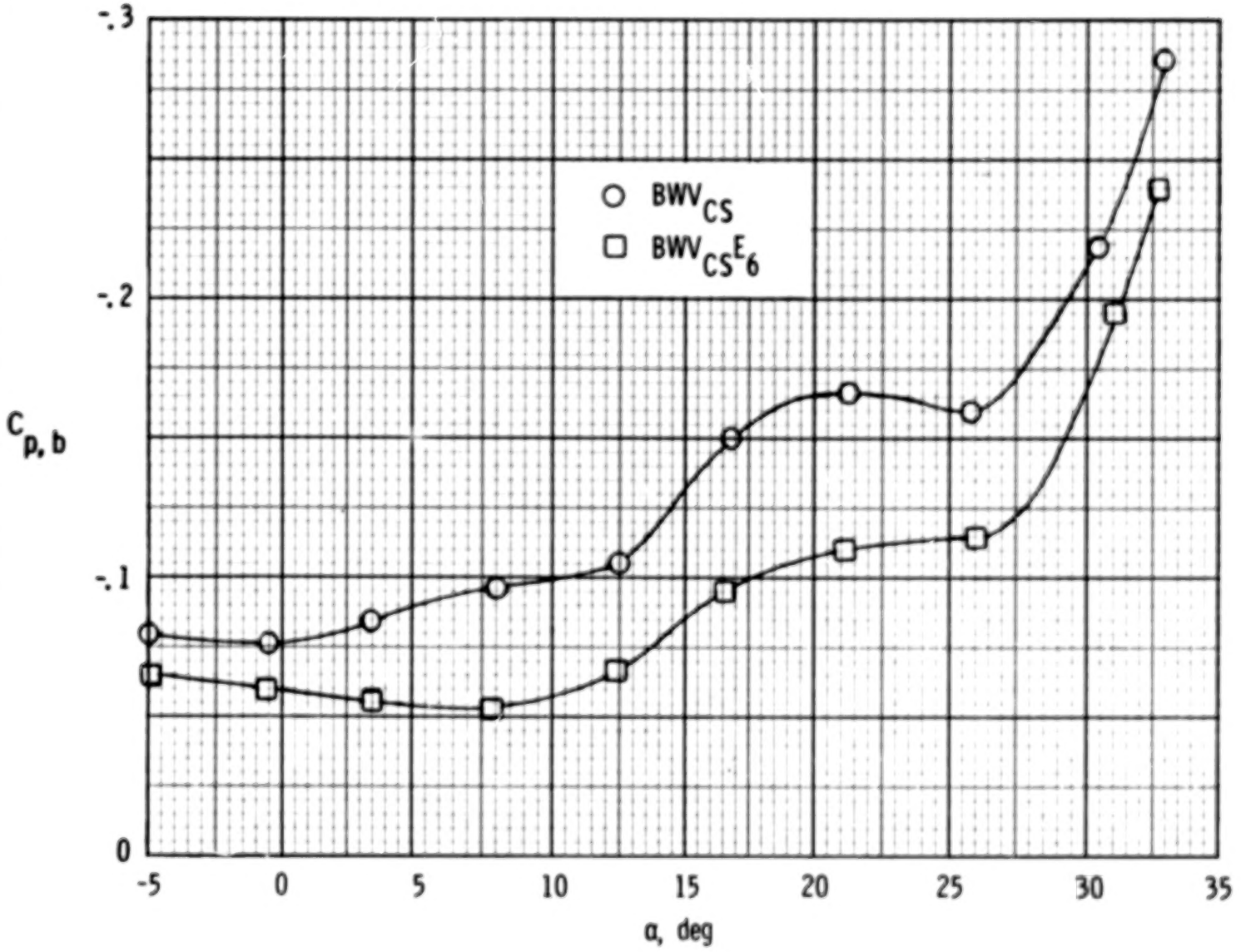

Figure 4.- Typical variation of measured base pressure coefficients with angle of attack; $R_\ell = 11.5 \times 10^6$.

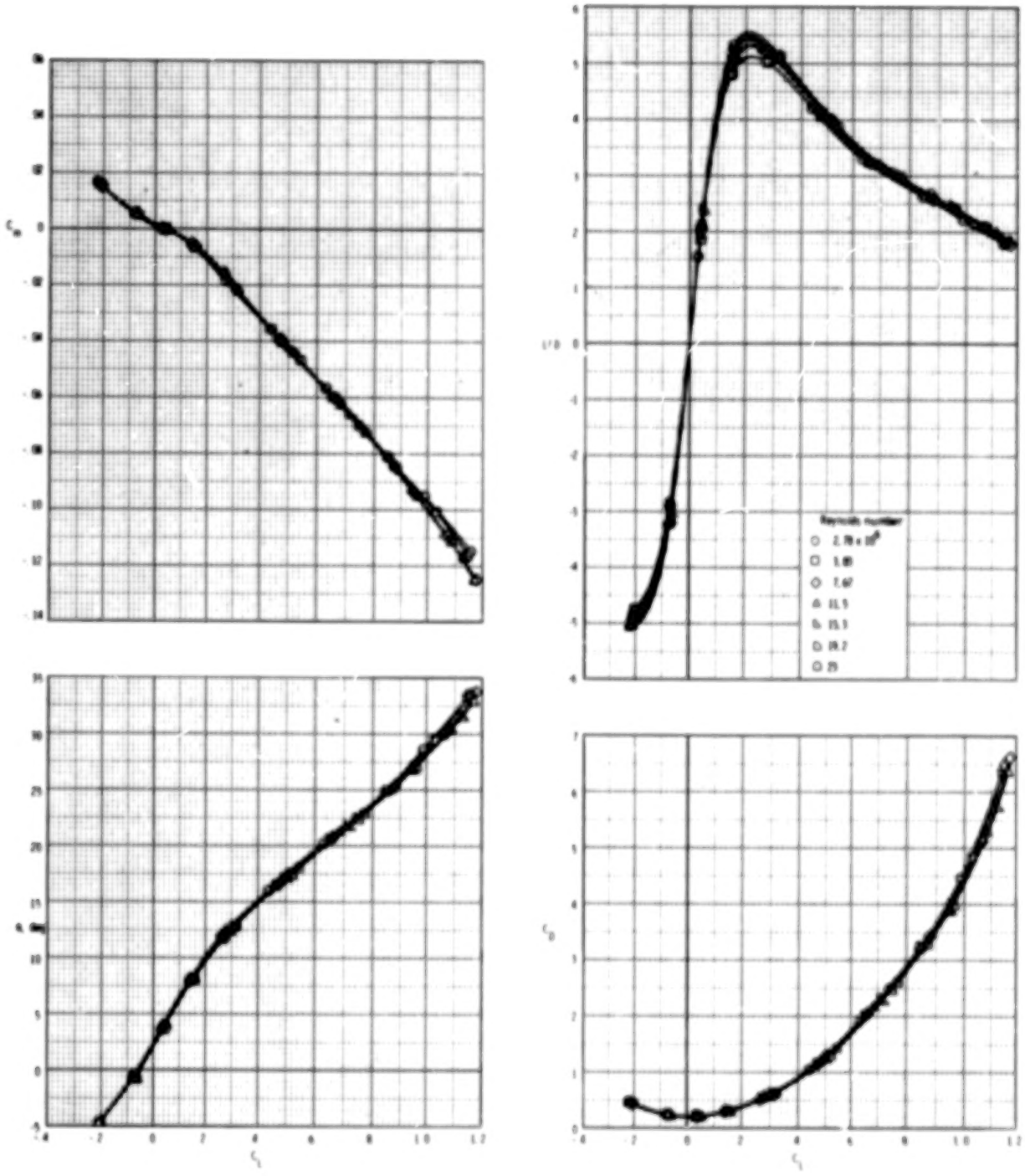

(a) BWV_{CS}.

Figure 5.- Variation of longitudinal aerodynamic characteristics with Reynolds number.

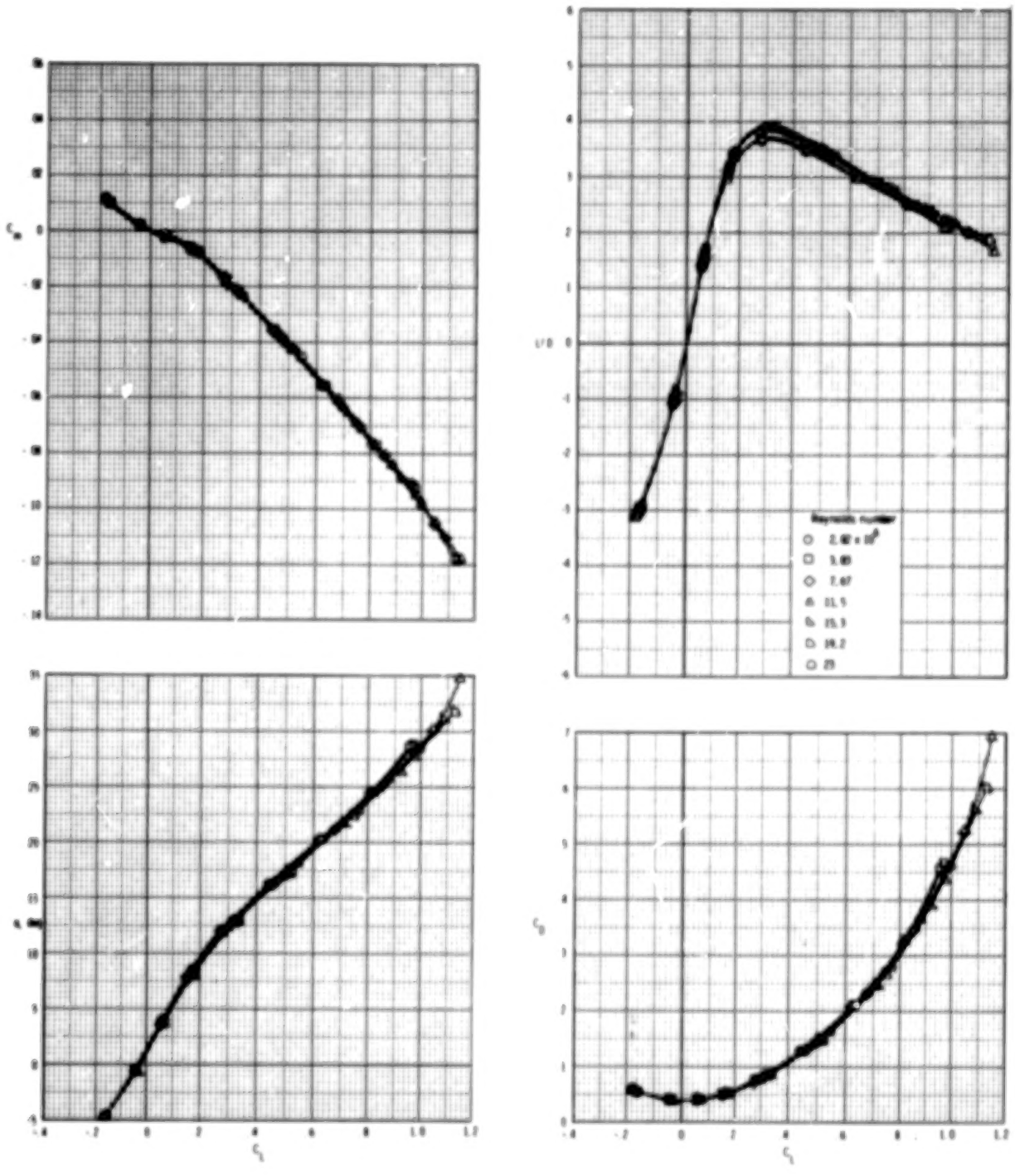

(b) $BWV_{CS}E_6$.

Figure 5.- Concluded.

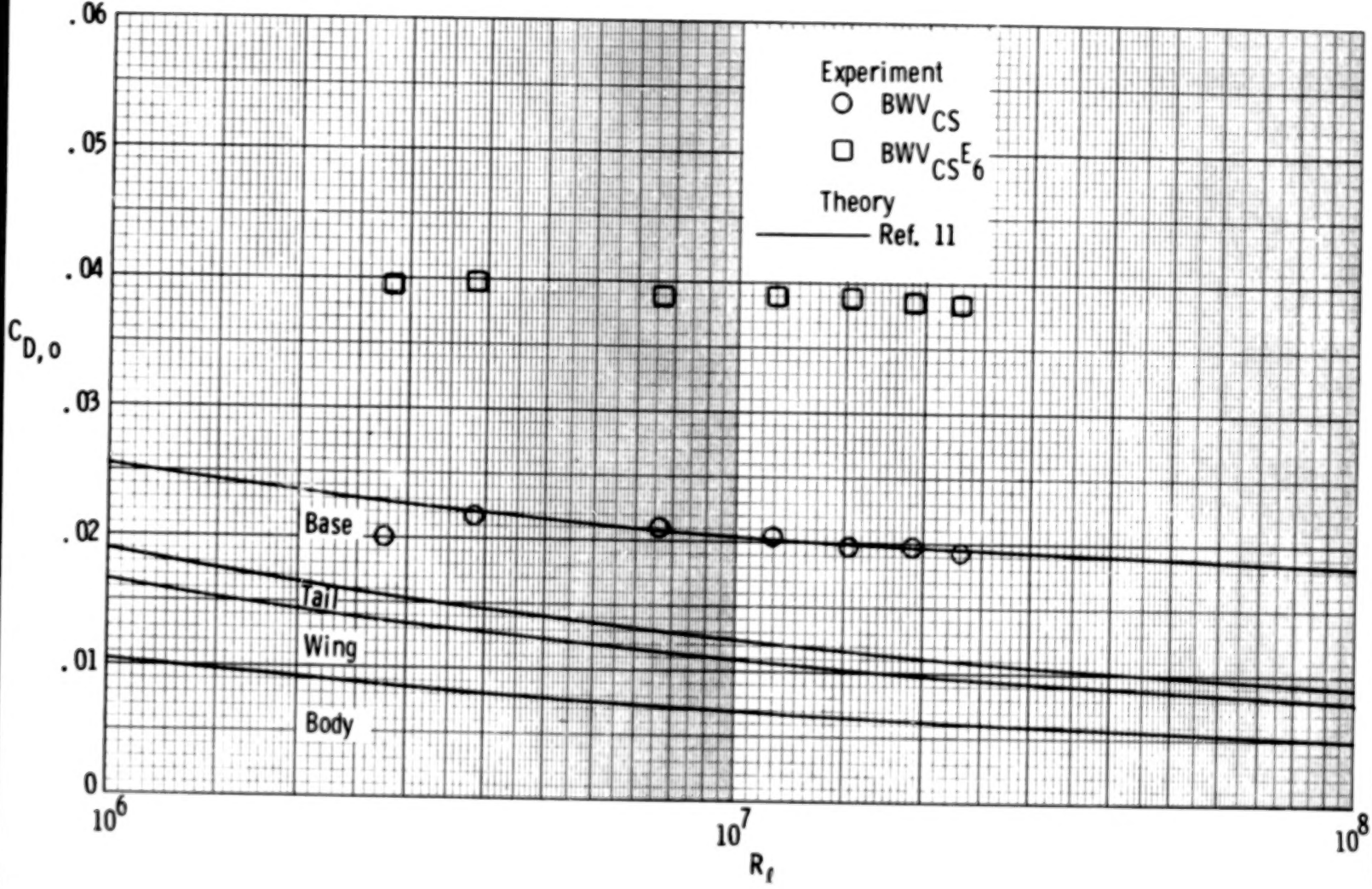

Figure 6.- Variation of $C_{D,o}$ with Reynolds number.

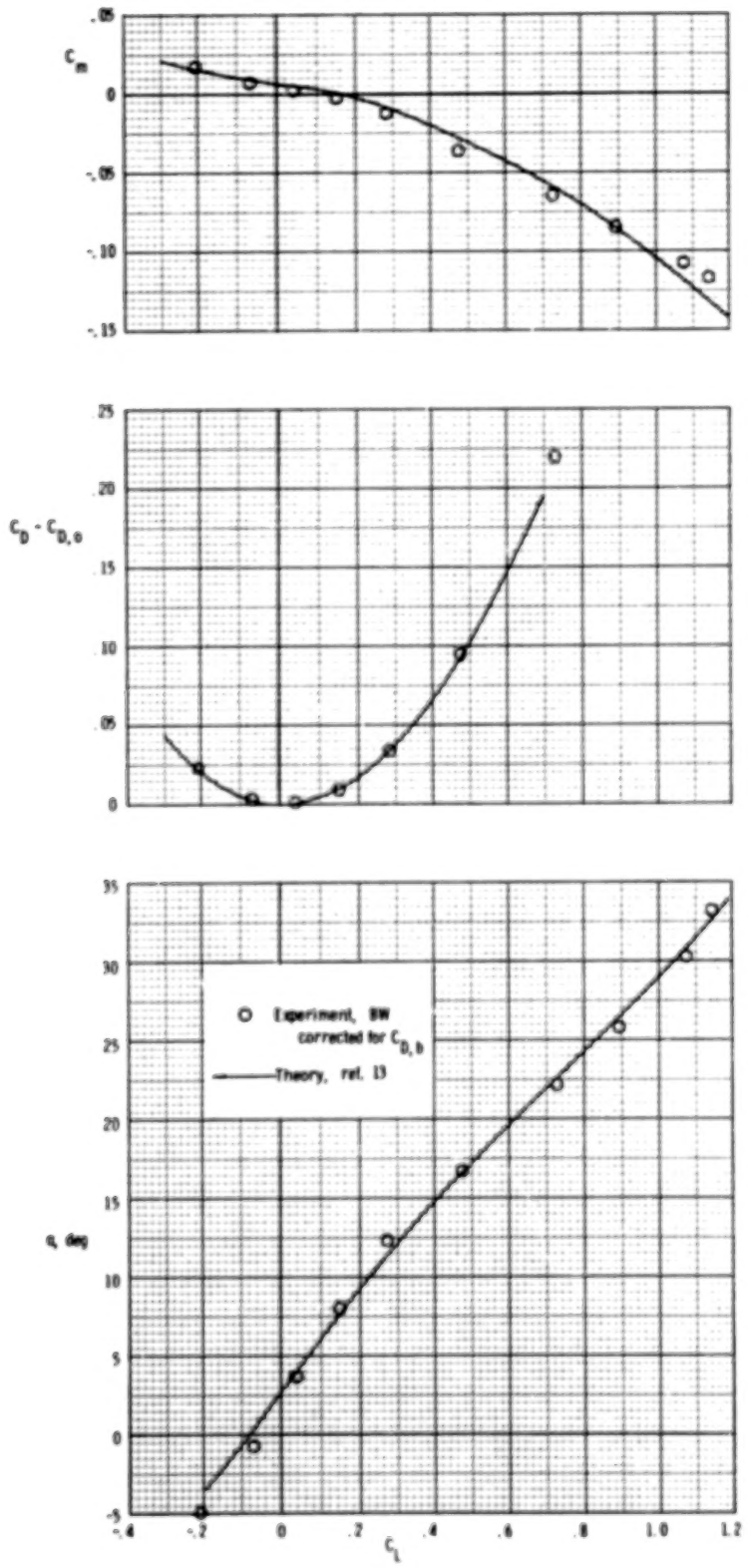

Figure 7.- Comparison of experiment with theory for body-wing configuration BW only; data corrected for $C_{D,b}$; $R_\ell = 11.5 \times 10^6$.

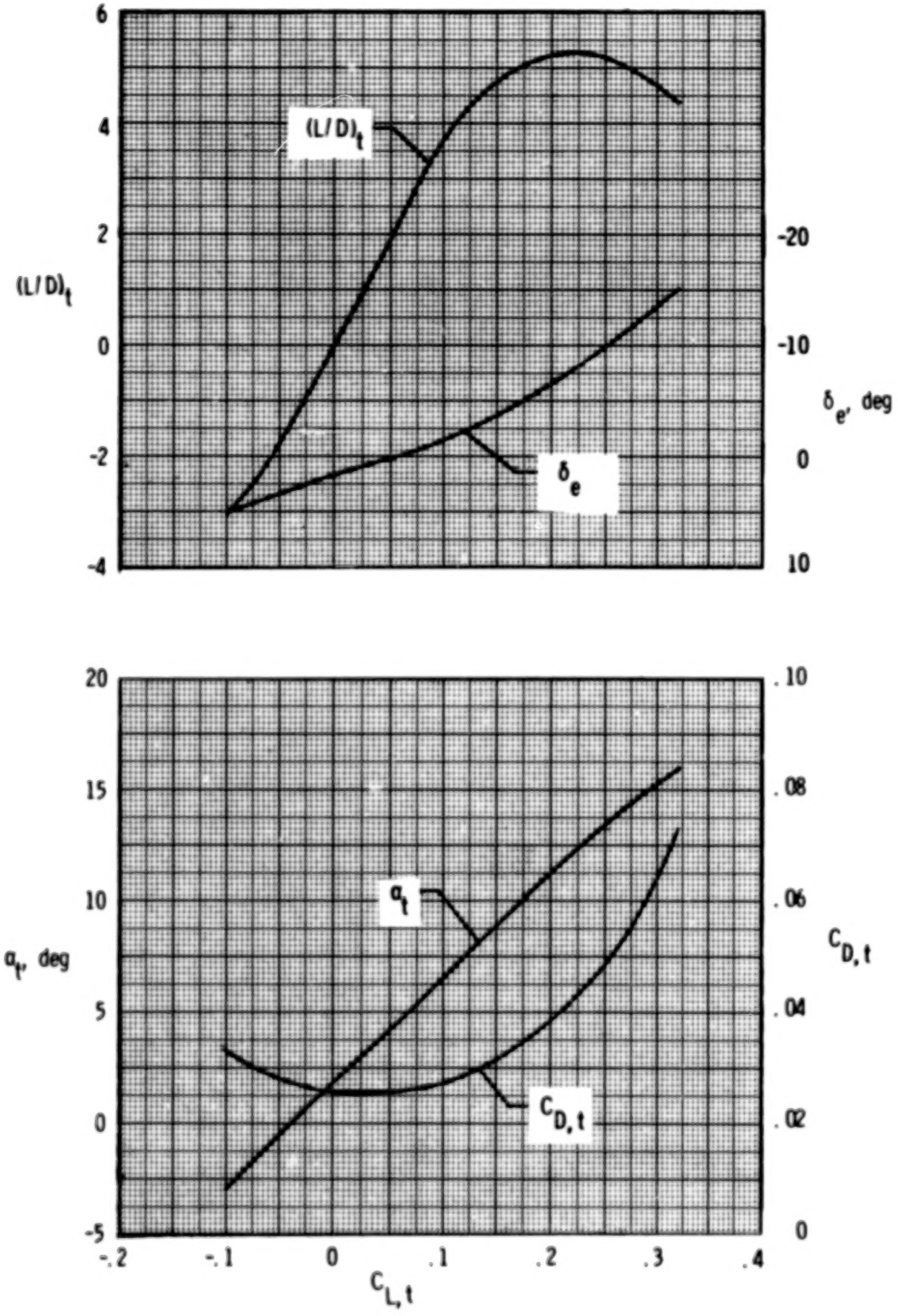

Figure 8.- Longitudinal aerodynamic characteristics at trim of BWV_{CS} configuration; $R_\ell = 11.5 \times 10^6$.

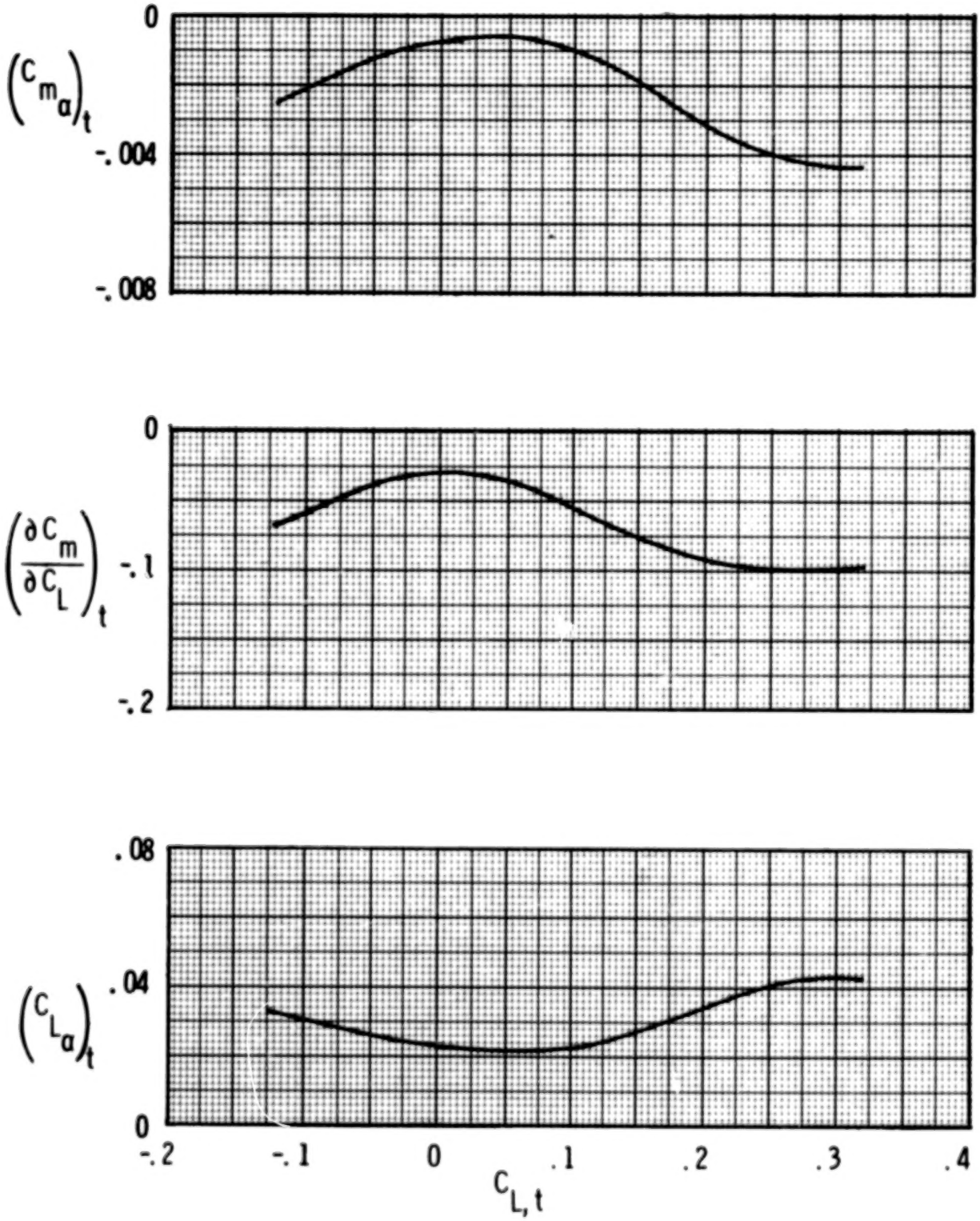

Figure 8.- Concluded.

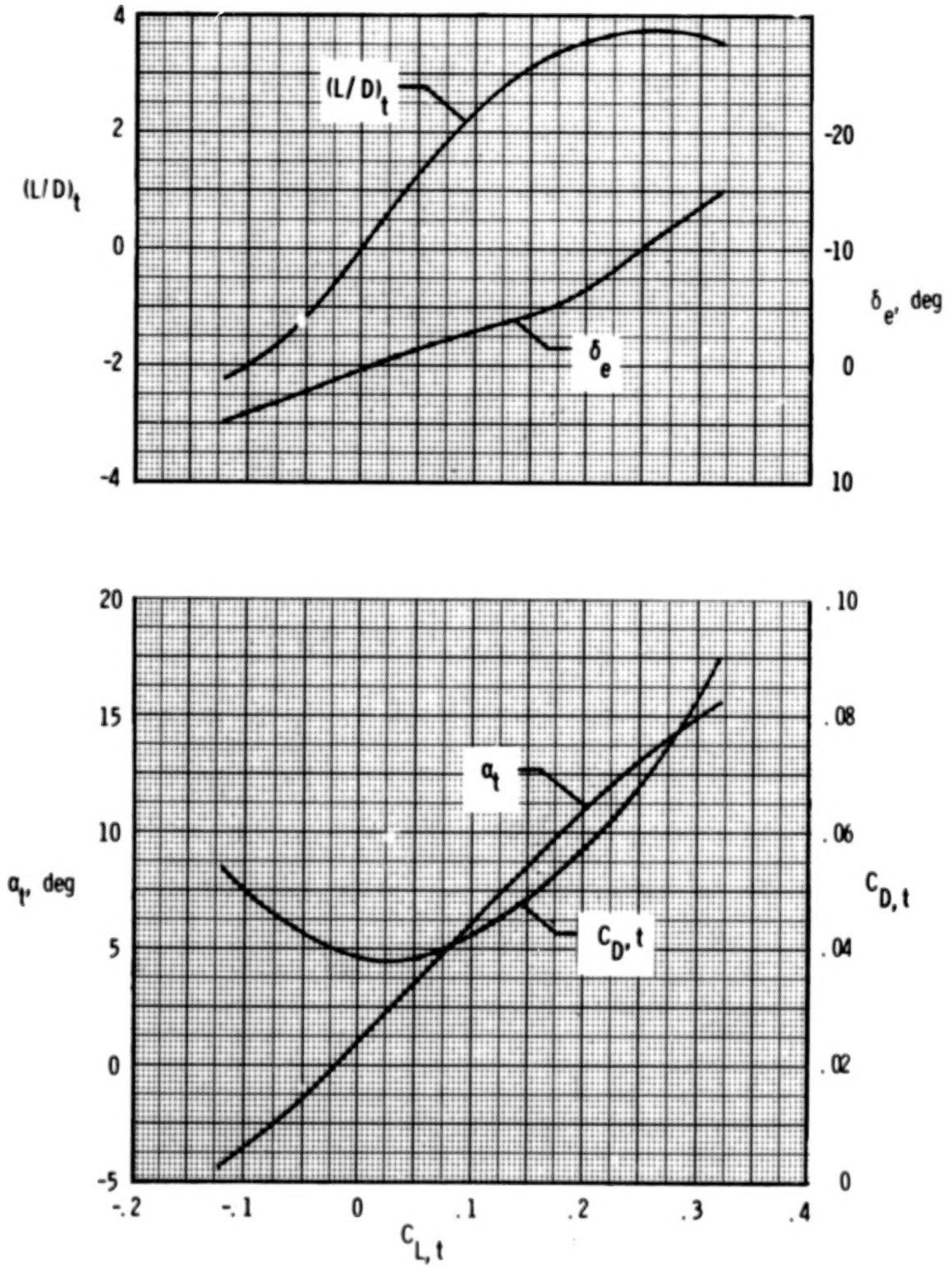

Figure 9.- Longitudinal aerodynamic characteristics at trim of $BWV_{CS}E_6$ configuration; $R_\ell = 11.5 \times 10^6$.

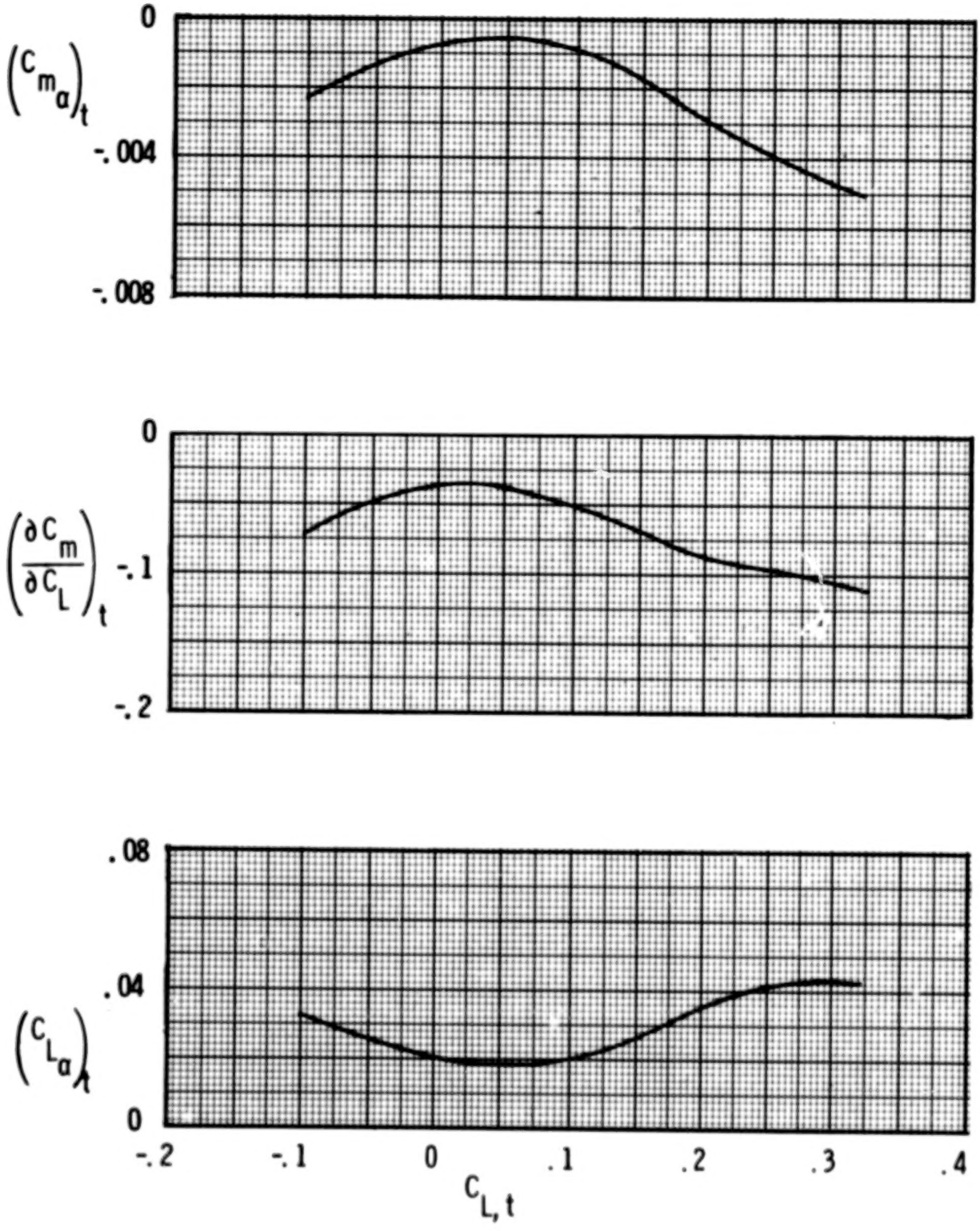

Figure 9.- Concluded.

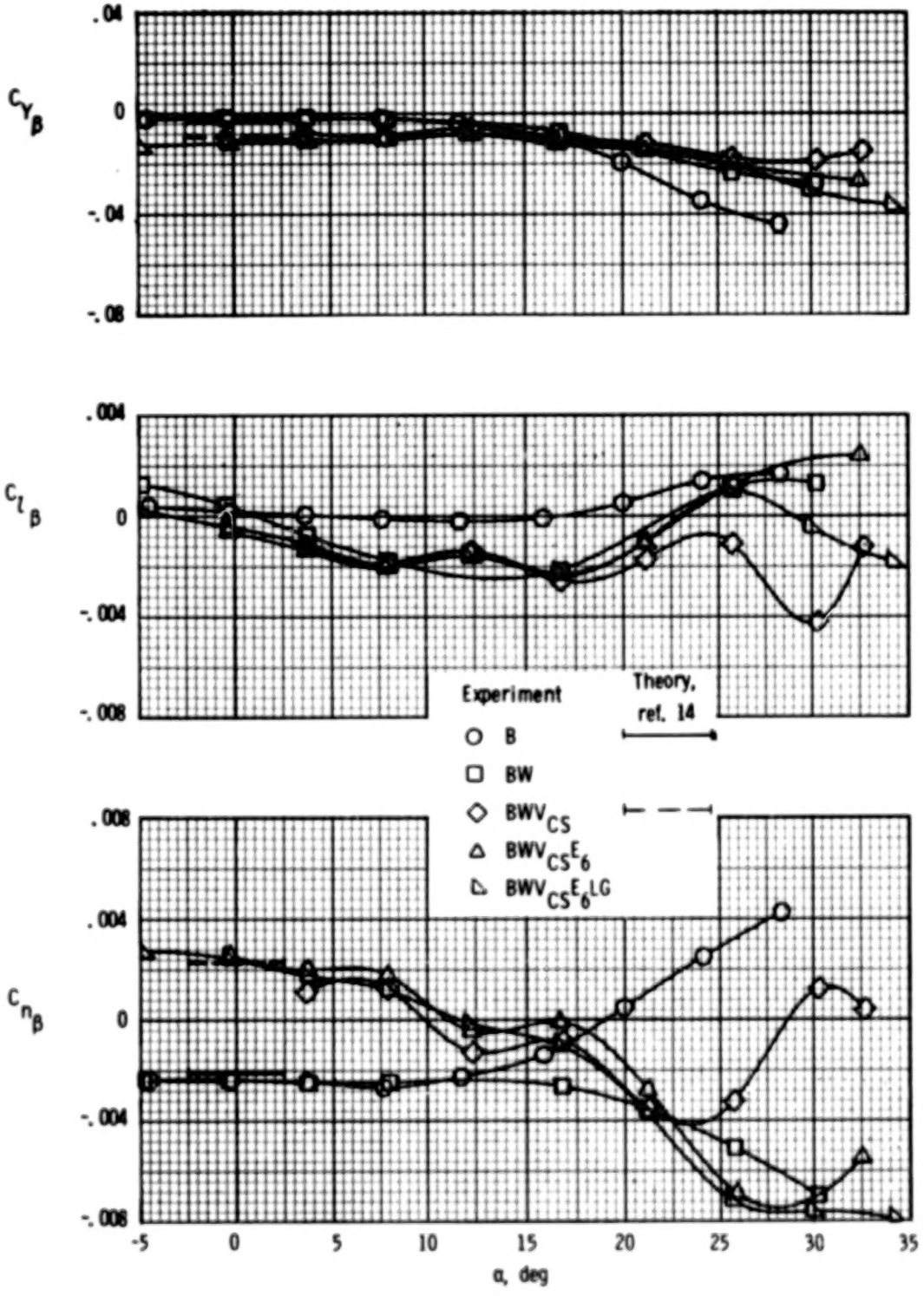

Figure 10.- Effect of body buildup on static lateral-directional stability characteristics; $R_\ell = 11.5 \times 10^6$.

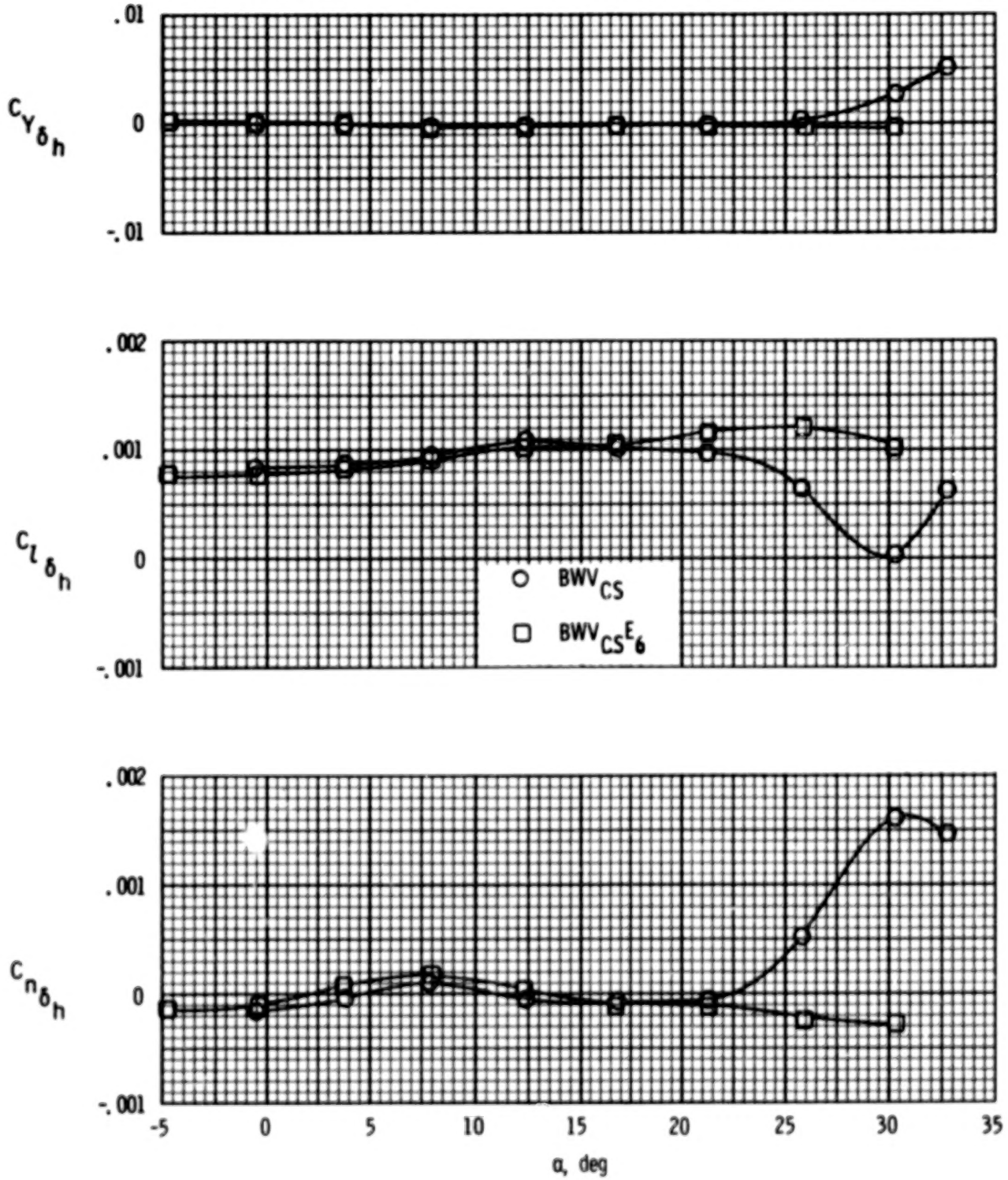

Figure 11.- Roll-control characteristics for basic BWV_{CS} and complete $BWV_{CS}E_6$ configurations; $R_\ell = 11.5 \times 10^6$.

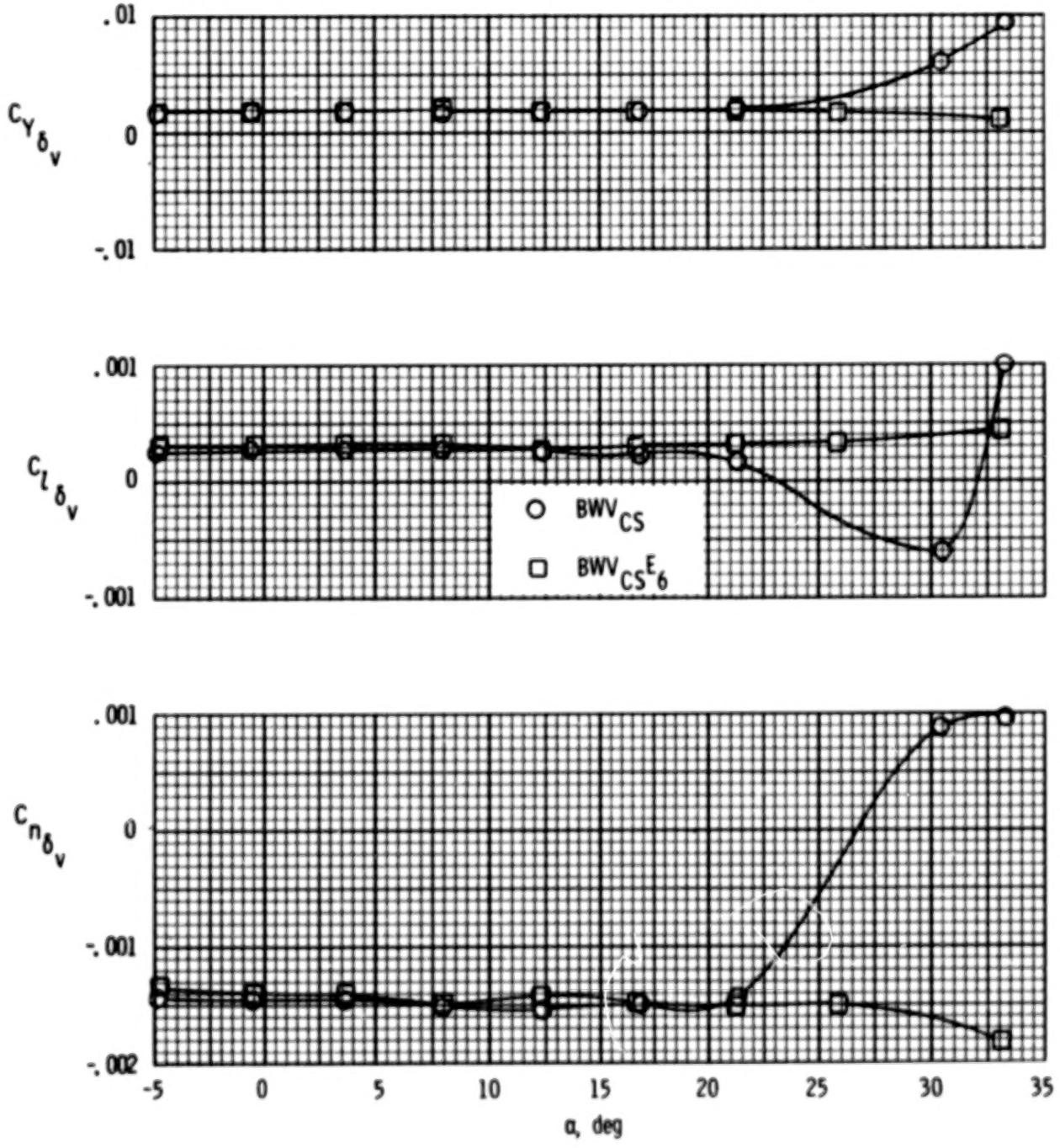

Figure 12.- Yaw-control characteristics for basic BWV_{CS} and complete $BWV_{CS}E_6$ configurations; $R_\ell = 11.5 \times 10^6$.

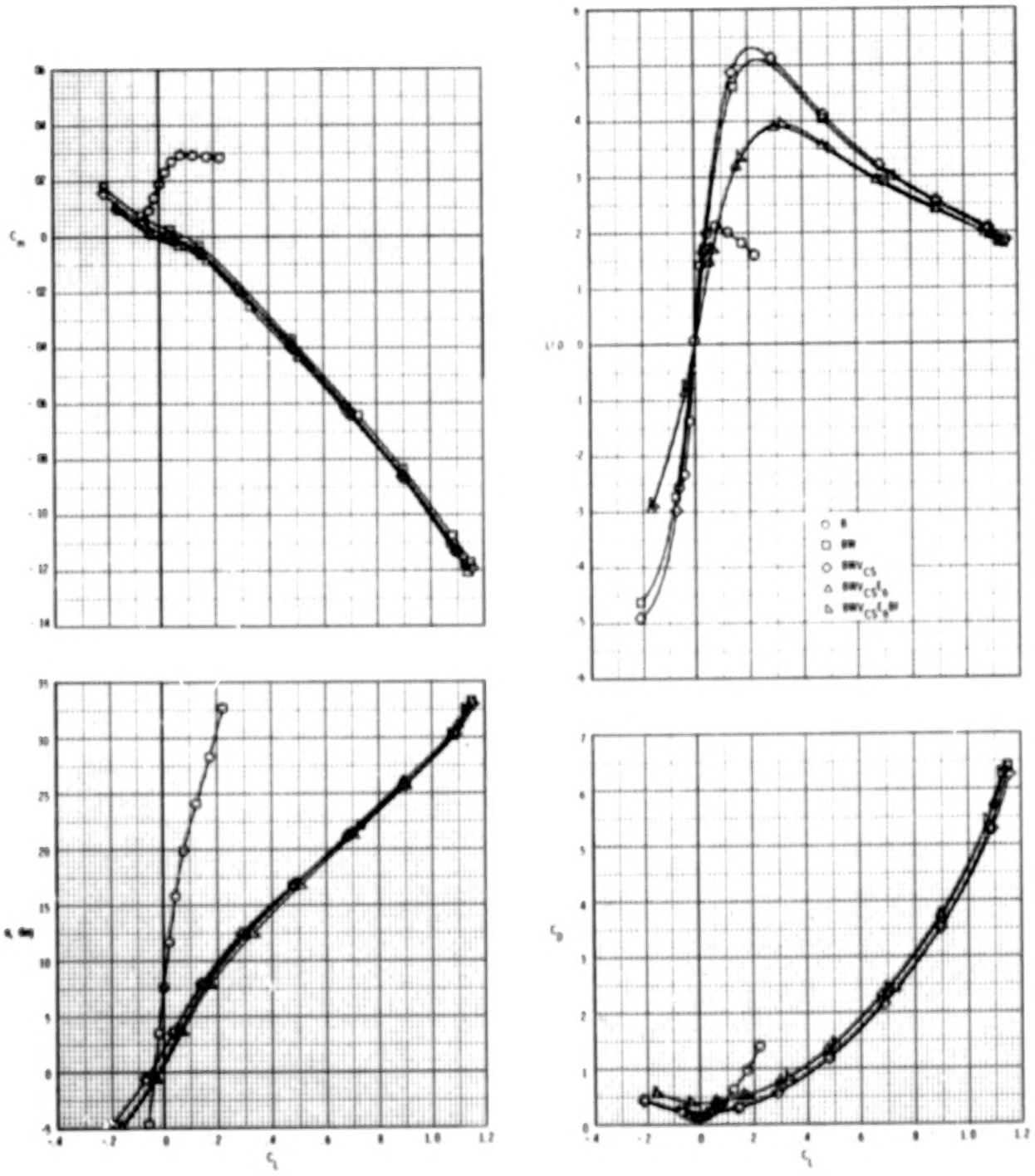

Figure 13.- Effect of body buildup on longitudinal aerodynamic characteristics; $R_{\ell} = 11.5 \times 10^6$.

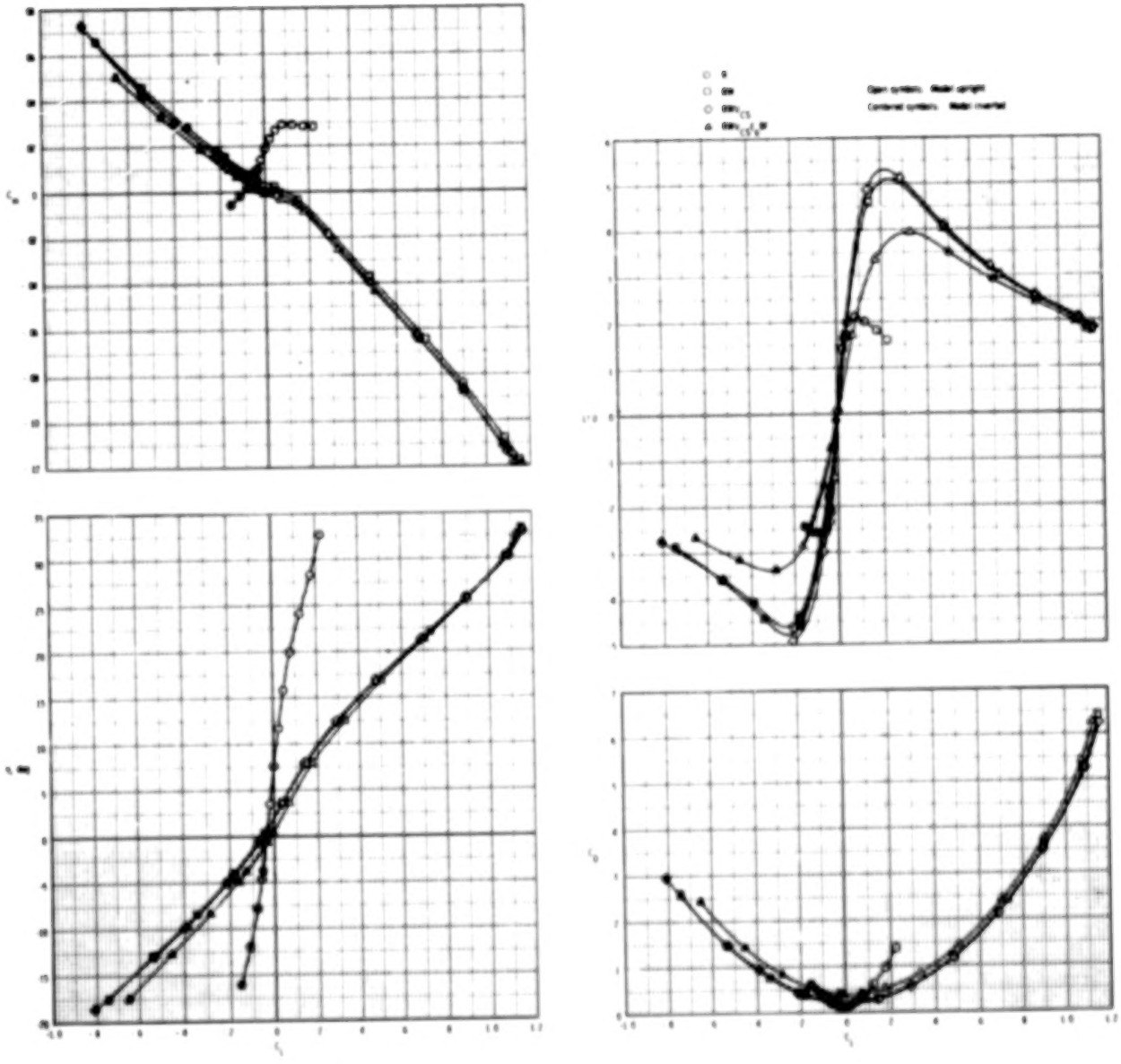

Figure 14.- Longitudinal aerodynamic characteristics for configurations upright and inverted; $R_\ell = 11.5 \times 10^6$.

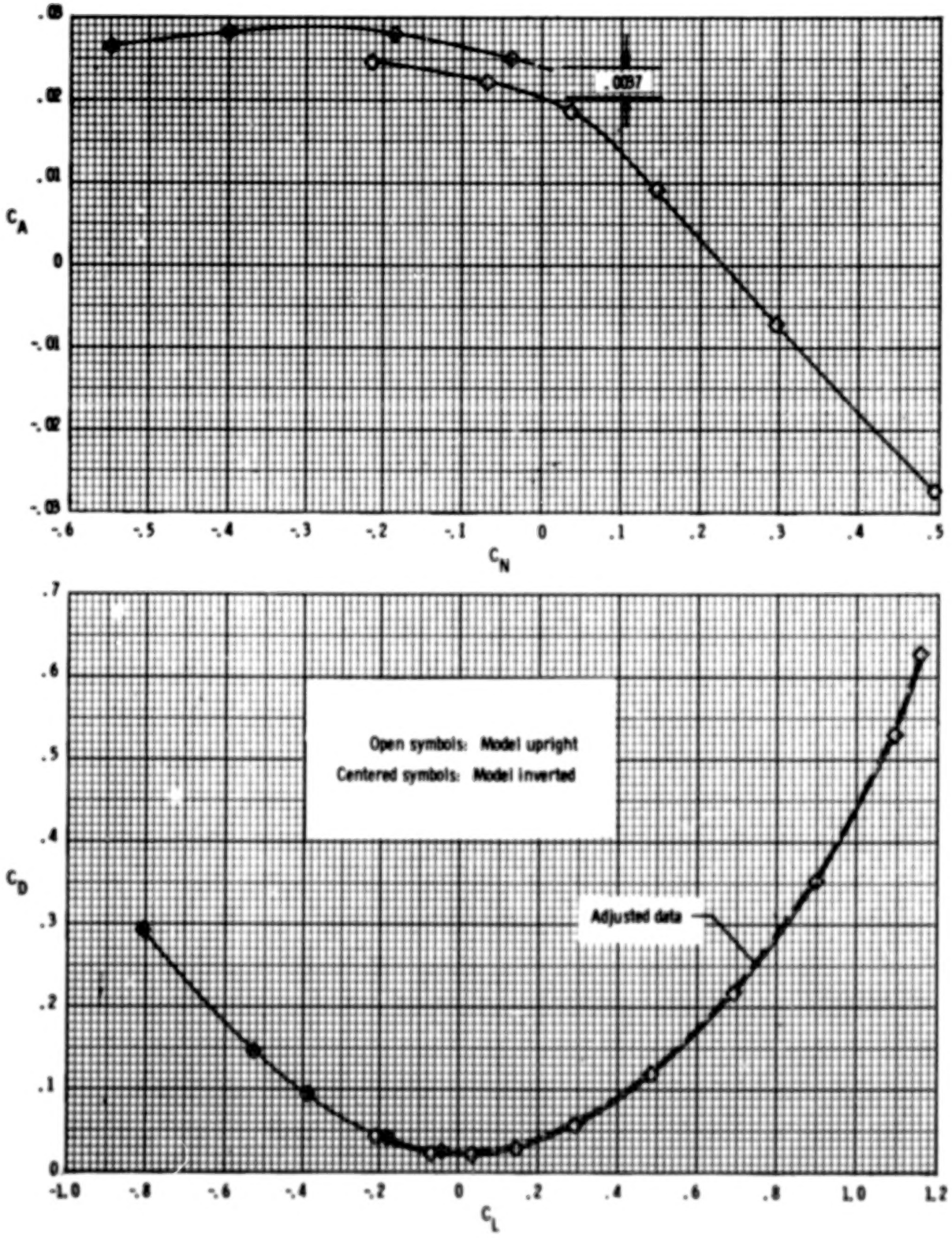

Figure 15.- Lift-drag polar and axial-normal force curve for BWV_{CS} configuration upright and inverted; $R_\ell = 11.5 \times 10^6$.

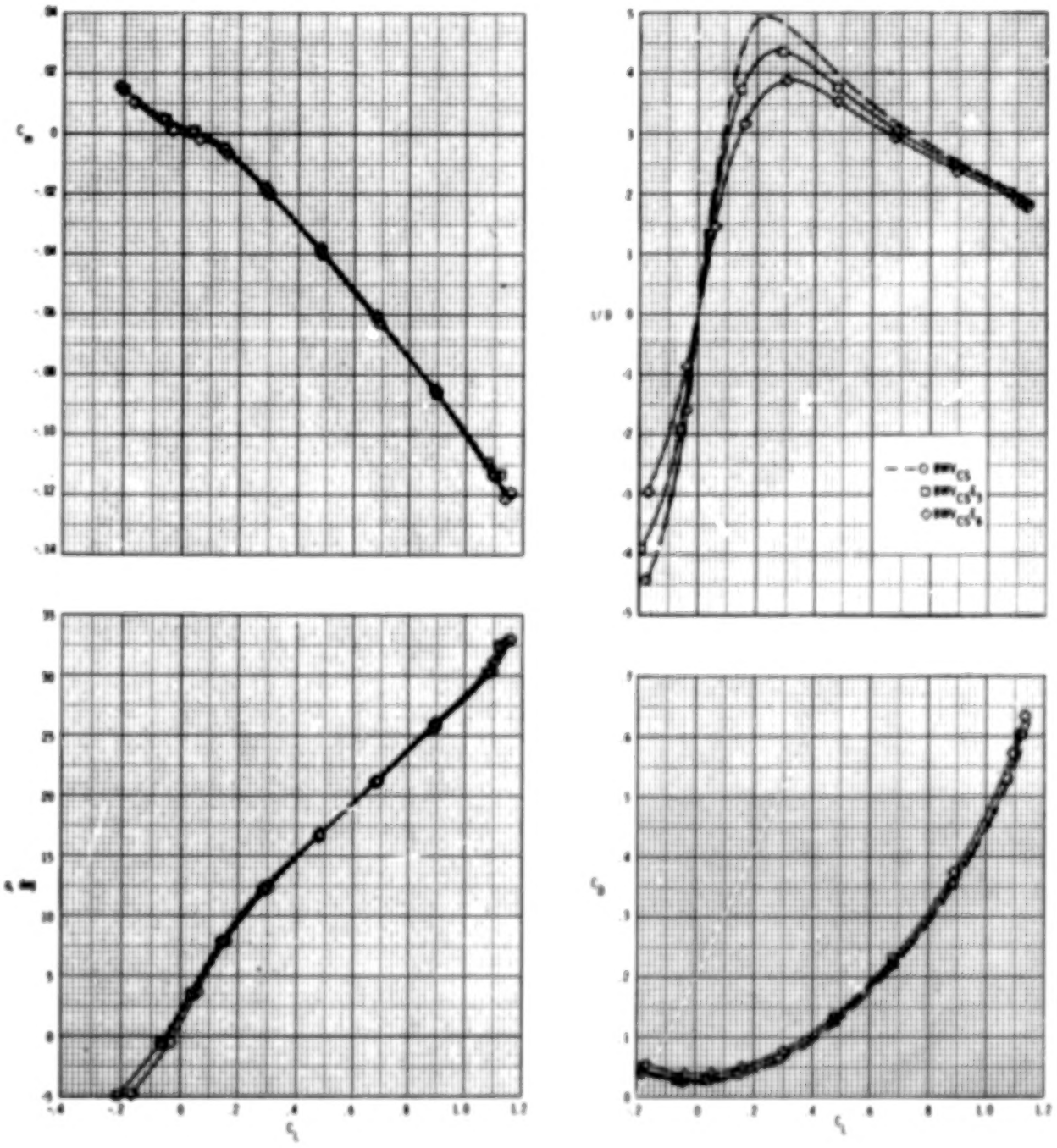

Figure 16.- Effect of number of scramjet engine modules on longitudinal aerodynamic characteristics; $R_{\ell} = 11.5 \times 10^6$.

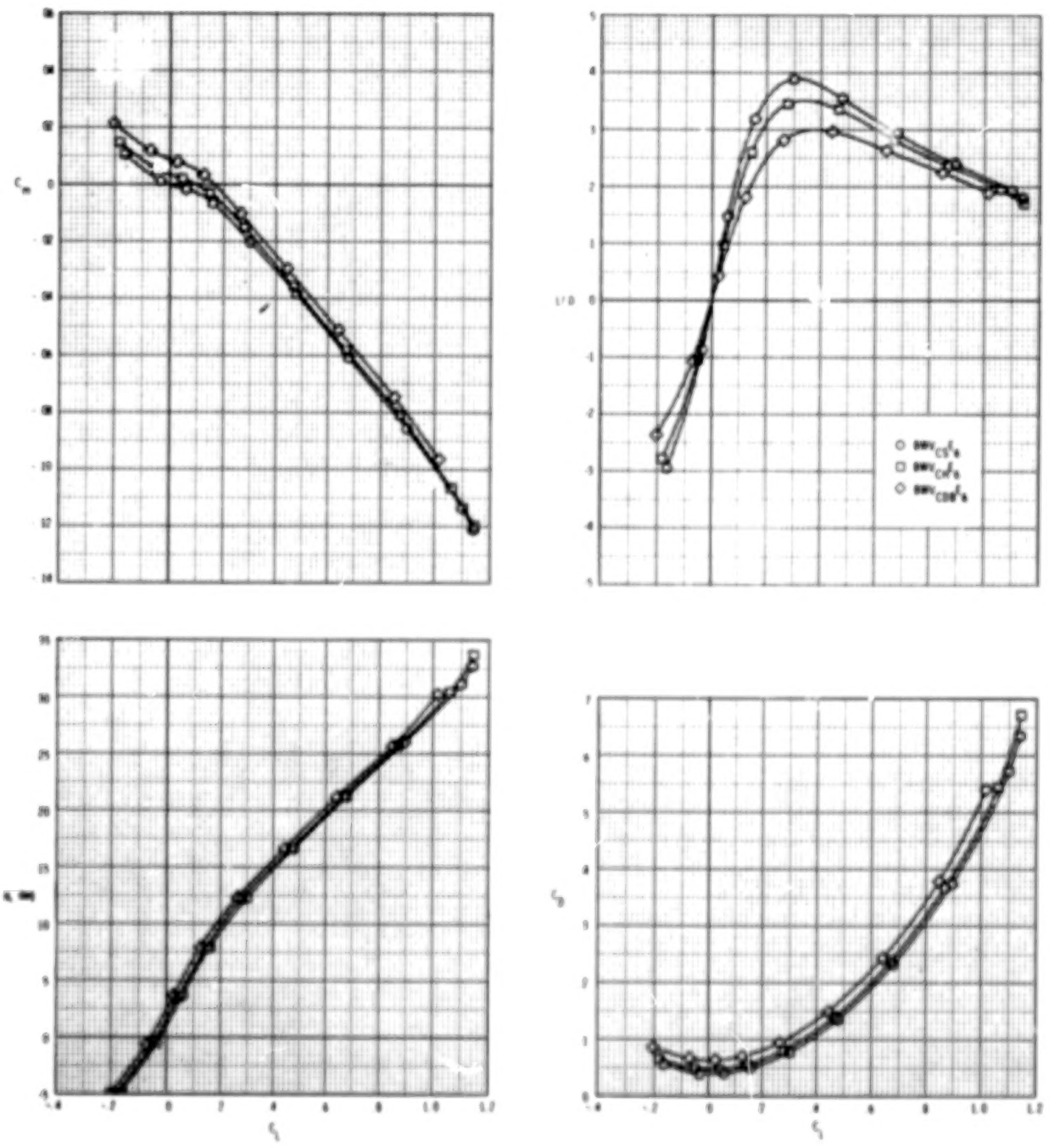

Figure 17.- Effect of vertical-tail variations on longitudinal aerodynamic characteristics; $R_{\ell} = 11.5 \times 10^6$.

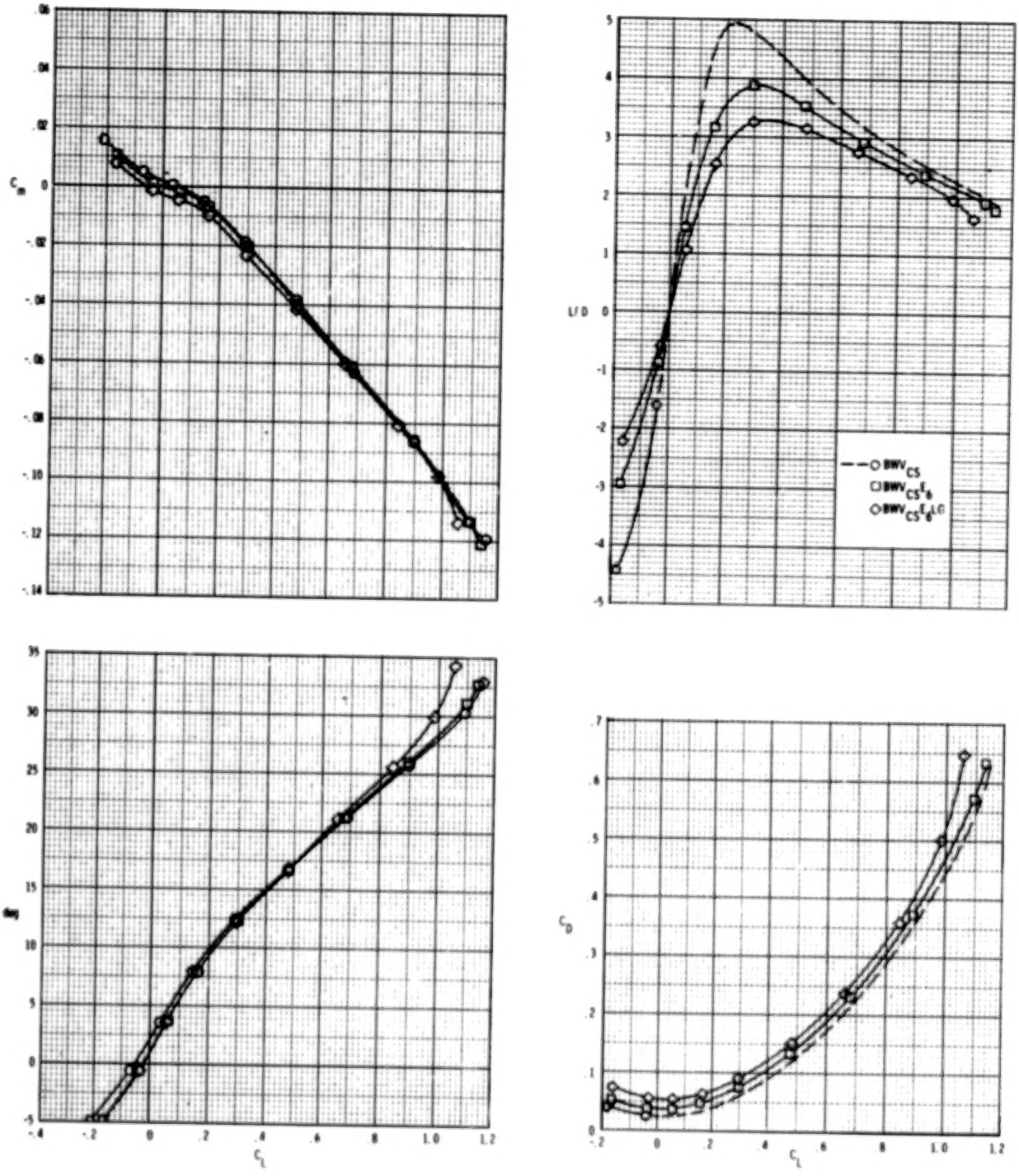

Figure 18.- Effect of landing-gear deployment on longitudinal aerodynamic characteristics; $R_\ell = 11.5 \times 10^6$.

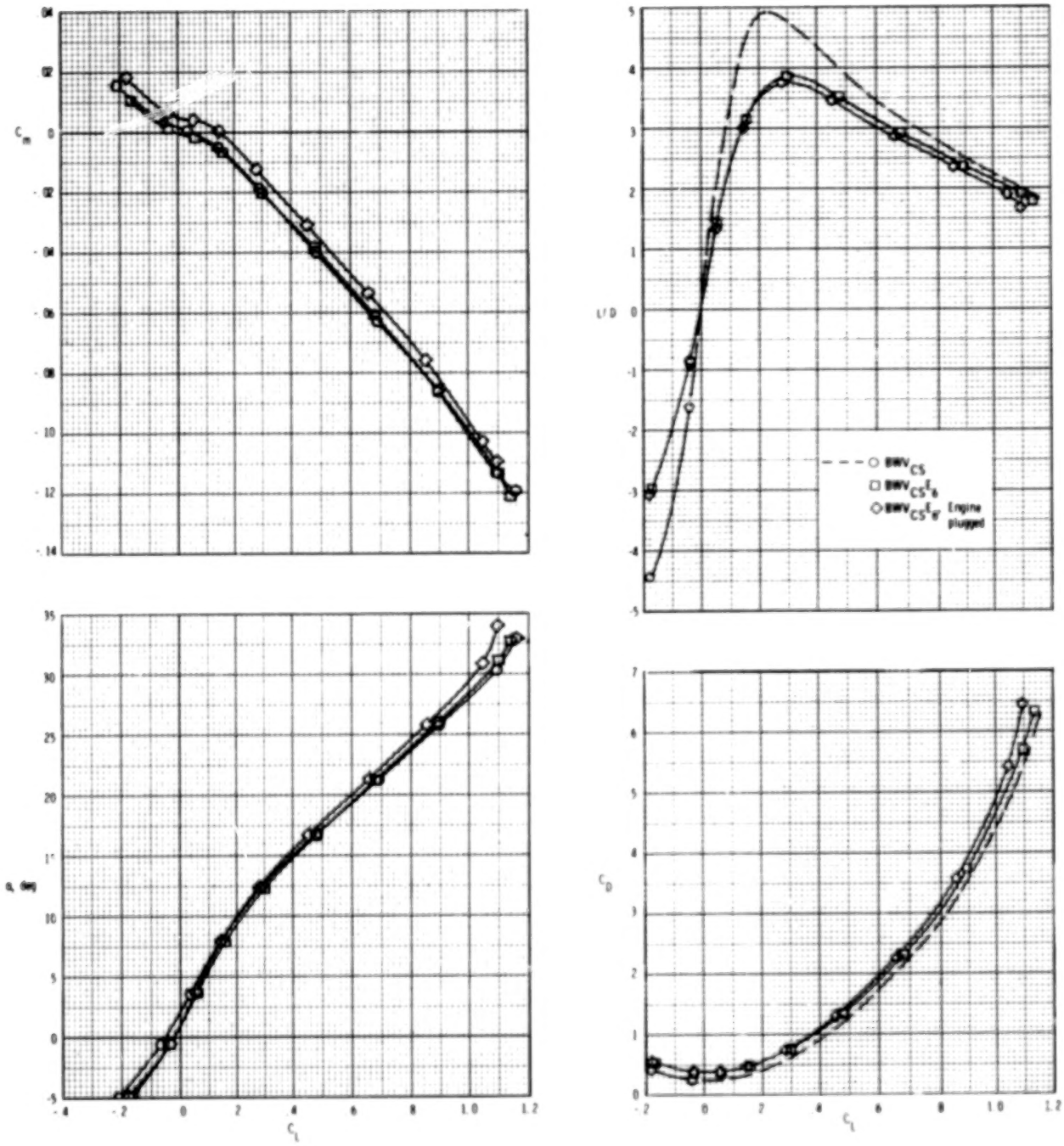

Figure 19.- Effect of plugging six-module scramjet engine on longitudinal aerodynamic characteristics; $R_\ell = 11.5 \times 10^6$.

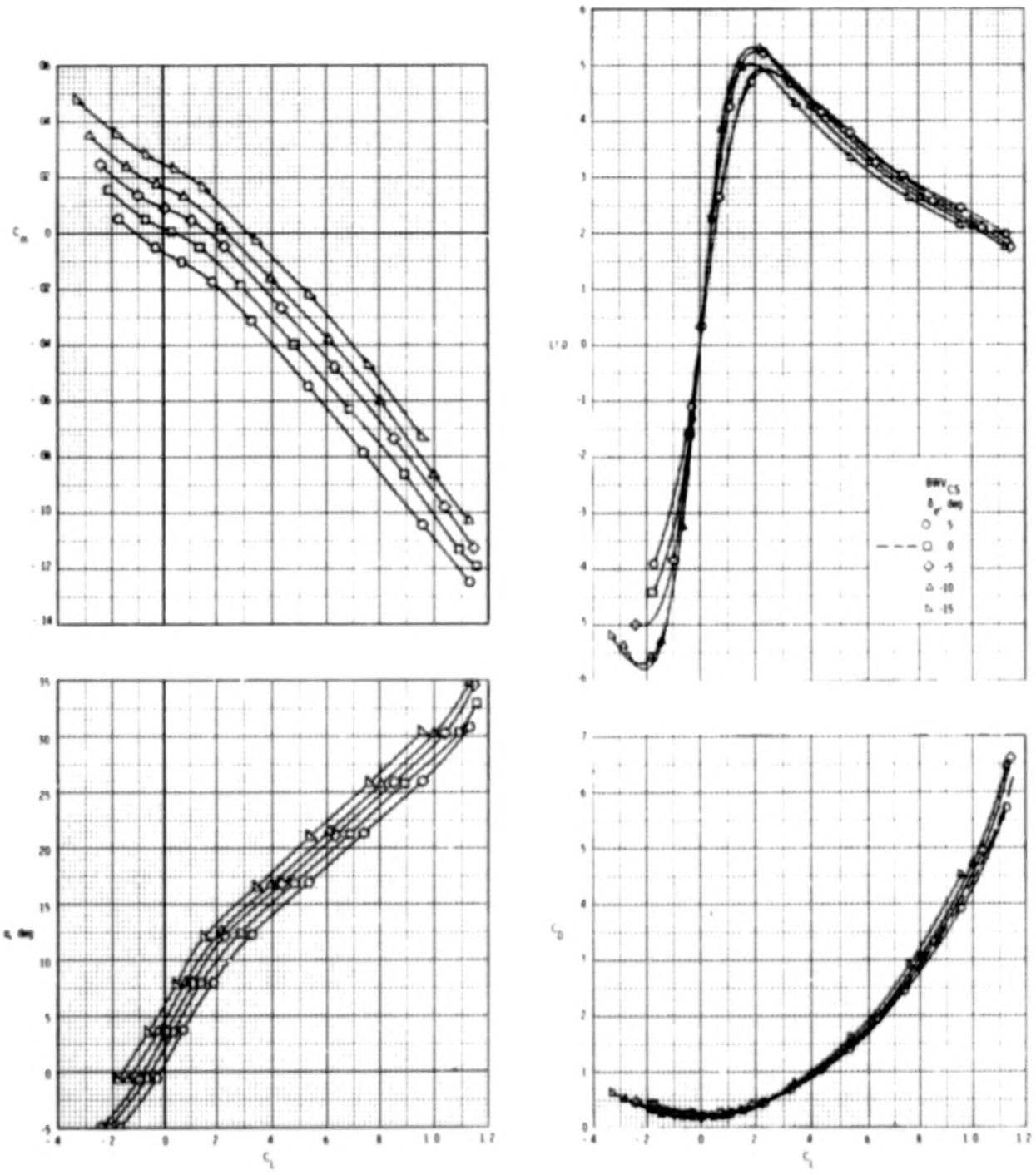

(a) BWV_{CS}.

Figure 20.- Effect of elevon deflection on longitudinal aerodynamic characteristics; $R_\ell = 11.5 \times 10^6$.

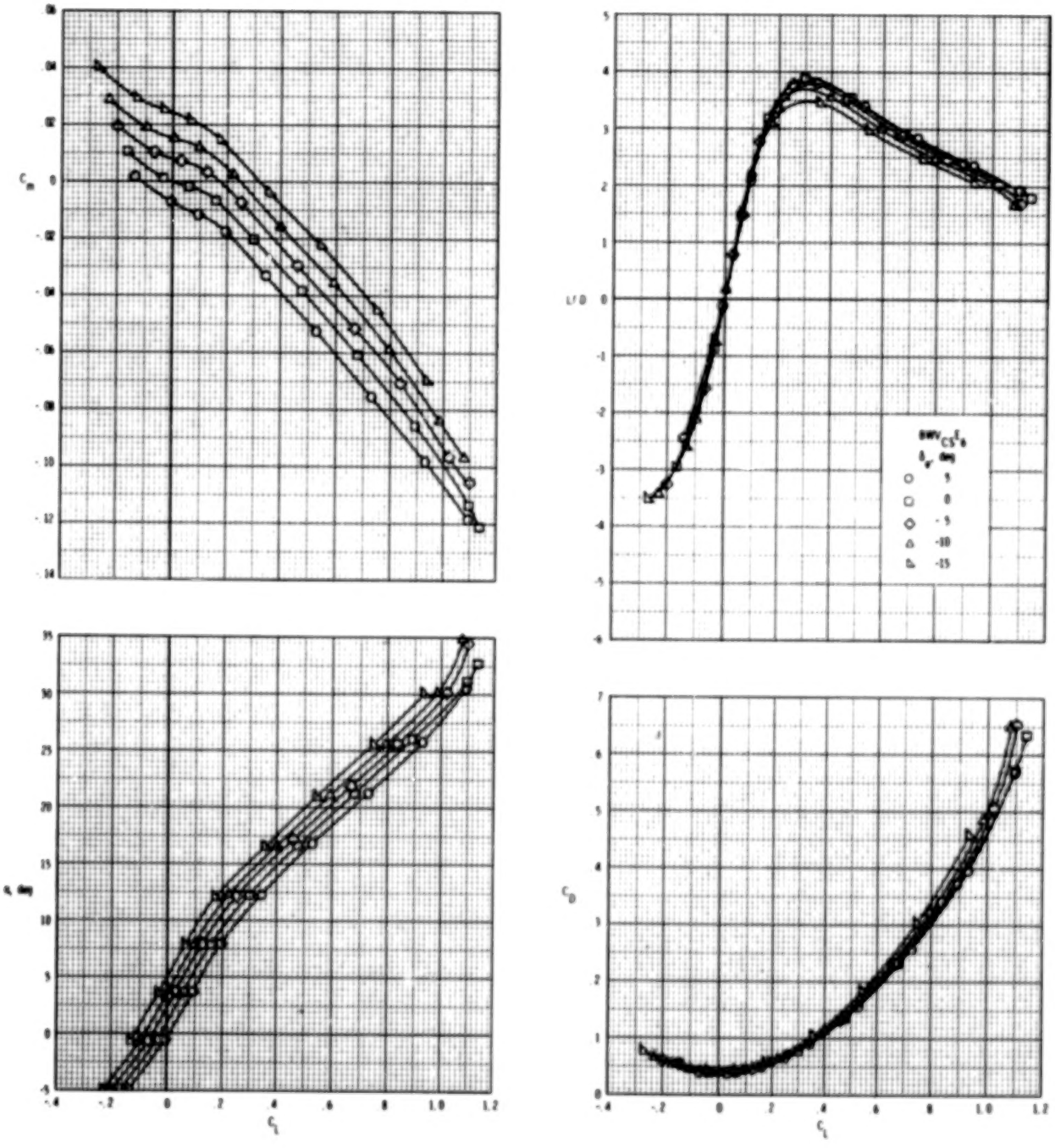

(b) $BWV_{CS}E_6$.

Figure 20.- Concluded.

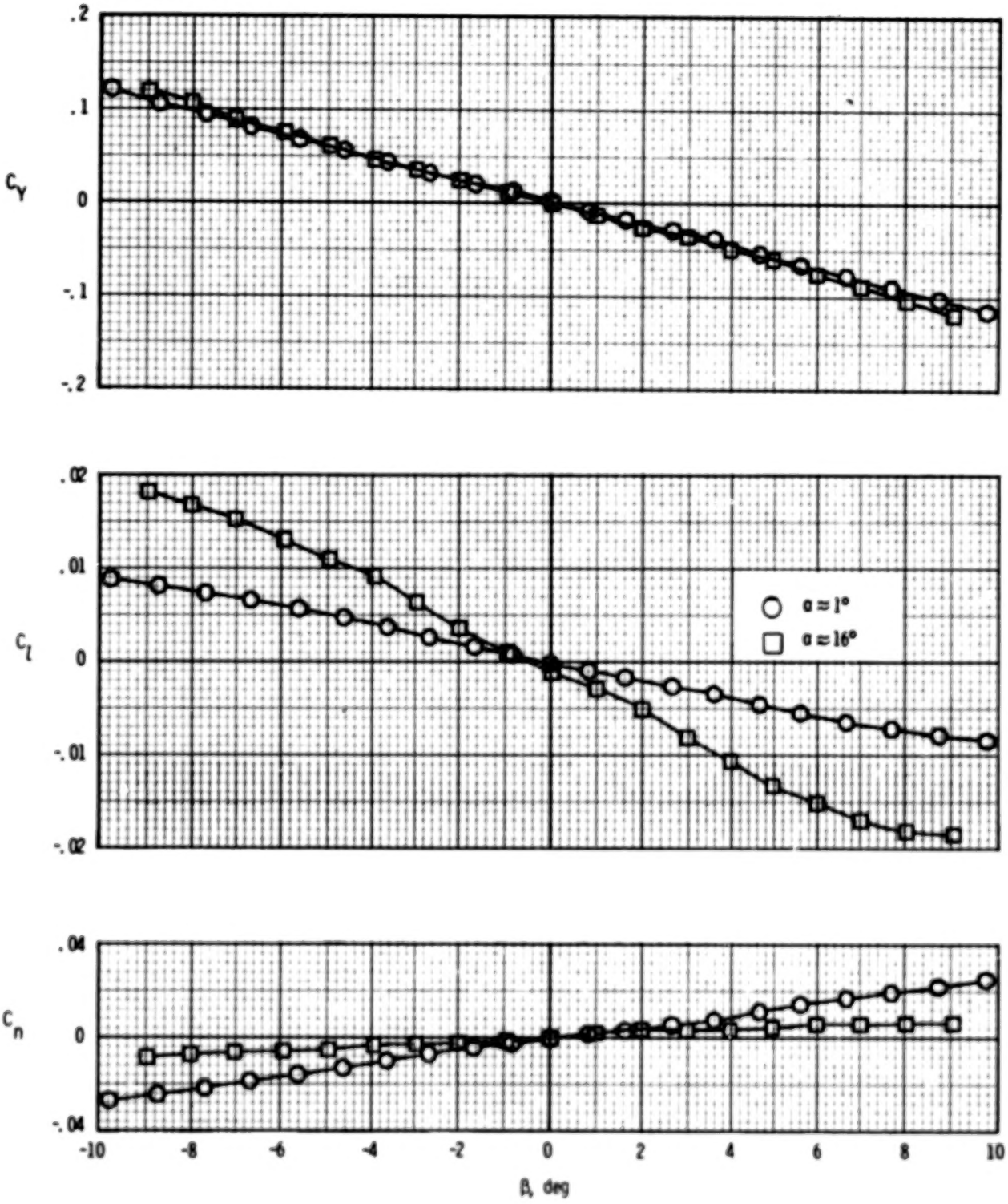

Figure 21.- Sideslip characteristics for complete configuration $BWV_{CS}E_6$ at $\alpha \approx 1^\circ$ and $\alpha \approx 16^\circ$; $R_\ell = 11.5 \times 10^6$.

1. Report No.	2. Government Accession No.	3. Recipient's Catalog No.
NASA TP-1189		

4. Title and Subtitle	5. Report Date
AERODYNAMIC CHARACTERISTICS AT MACH NUMBER 0.2 OF A WING-BODY CONCEPT FOR A HYPERSONIC RESEARCH AIRPLANE	June 1978
	6. Performing Organization Code
7. Author(s)	8. Performing Organization Report No.
James L. Dillon and Theodore R. Creel, Jr.	L-12063
	10. Work Unit No.
9. Performing Organization Name and Address	505-11-33-00
NASA Langley Research Center Hampton VA 23665	11. Contract or Grant No.
	13. Type of Report and Period Covered
12. Sponsoring Agency Name and Address	Technical Paper
National Aeronautics and Space Administration Washington, DC 20546	14. Sponsoring Agency Code

15. Supplementary Notes

16. Abstract

An experimental investigation of the static aerodynamic characteristics of a model of a wing-body concept for a high-speed research airplane was conducted in the Langley low-turbulence pressure tunnel. The experiment consisted of configuration buildup from the basic body by adding a wing, center vertical tail, three-module scramjet, and six-module scramjet engine. The test Mach number was 0.2 at Reynolds numbers, based on fuselage length, ranging from 2.78×10^6 to 23×10^6. The test angle-of-attack range was approximately -5° to 30° at constant angles of sideslip of 0° and 4°. The elevons were deflected from 5° to -15°. Roll and yaw control were investigated.

17. Key Words (Suggested by Author(s))	18. Distribution Statement
Aerodynamics Subsonic performance stability and control Hypersonic configuration	Unclassified - Unlimited Subject Category 02

19. Security Classif. (of this report)	20. Security Classif. (of this page)	21. No. of Pages	22. Price*
Unclassified	Unclassified	45	$4.50

* For sale by the National Technical Information Service, Springfield, Virginia 22161

NASA-Langley, 1978